the deubiquitinase activity of USP7 to stabilize ERCC6 in TCR. We conclude that the UVSSA-USP7 complex has an important role in TCR, whereby it controls the steady-state levels of ERCC6.

METHODS

Methods and any associated references are available in the online version of the paper at http://www.nature.com/naturegenetics/.

Note: Supplementary information is available on the Nature Genetics website.

ACKNOWLEDGMENTS

We thank Y. Iwamoto and I. Kuraoka for their help in DNA sequencing and microcell-mediated chromosome transfer and M. Hoshi for her help in establishing Flp-In cells and performing immunoprecipitation. We also thank M. Yamaizumi (Kumamoto University Medical School) and N.G. Jaspers (Erasmus Medical Centre) for providing Kps3 cells and TA-24 cells, respectively. We thank G. Spivak for critical reading of the manuscript. This work was supported by a Grant-in-Aid for Scientific Research on Innovative Areas from the Ministry of Education, Culture, Sports, Science and Technology (MEXT) of Japan and by Health and Labor Sciences Research Grants for Research on Intractable Diseases (to K.T.). Part of this work was carried out under the Cooperative Research Project Program of the Institute of Development, Aging and Cancer (IDAC) at Tohoku University.

AUTHOR CONTRIBUTIONS

X.Z., K.H., M.S. and K.T. conceived the experiments. K.T. and H.T. established the cell lines. X.Z., K.H. and C.I. performed microcell-mediated chromosome transfer. A.U., K.H. and M.H. performed CGH array analysis. X.Z., M.S. and S.K. performed biochemical analysis. E.G.N. diagnosed Cockayne syndrome patients. K.T., X.Z., K.H., M.S., M.H., T.N. and A.Y. analyzed the data. K.T., X.Z., M.S. and K.H. wrote the manuscript.

COMPETING FINANCIAL INTERESTS

The authors declare no competing financial interests.

Published online at http://www.nature.com/naturegenetics/.
Reprints and permissions information is available online at http://www.nature.com/reprints/index.html.

1. Hanawalt, P.C. & Spivak, G. Transcription-coupled DNA repair: two decades of progress and surprises. *Nat. Rev. Mol. Cell Biol.* **9**, 958–970 (2008).
2. Fousteri, M. & Mullenders, L.H. Transcription-coupled nucleotide excision repair in mammalian cells: molecular mechanisms and biological effects. *Cell Res.* **18**, 73–84 (2008).
3. Spivak, G. UV-sensitive syndrome. *Mutat. Res.* **577**, 162–169 (2005).
4. Itoh, T., Ono, T. & Yamaizumi, M. A new UV-sensitive syndrome not belonging to any complementation groups of xeroderma pigmentosum or Cockayne syndrome: siblings showing biochemical characteristics of Cockayne syndrome without typical clinical manifestations. *Mutat. Res.* **314**, 233–248 (1994).
5. Horibata, K. *et al.* Complete absence of Cockayne syndrome group B gene product gives rise to UV-sensitive syndrome but not Cockayne syndrome. *Proc. Natl. Acad. Sci. USA* **101**, 15410–15415 (2004).
6. Nardo, T. *et al.* A UV-sensitive syndrome patient with a specific *CSA* mutation reveals separable roles for CSA in response to UV and oxidative DNA damage. *Proc. Natl. Acad. Sci. USA* **106**, 6209–6214 (2009).
7. Nagase, T., Kikuno, R., Ishikawa, K., Hirosawa, M. & Ohara, O. Prediction of the coding sequences of unidentified human genes. XVII. The complete sequences of 100 new cDNA clones from brain which code for large proteins *in vitro*. *DNA Res.* **7**, 143–150 (2000).
8. Nicholson, B. & Suresh Kumar, K.G. The multifaceted roles of USP7: new therapeutic opportunities. *Cell Biochem. Biophys.* **60**, 61–68 (2011).
9. Sanford, J.A. & Stubblefield, E. General protocol for microcell-mediated chromosome transfer. *Somat. Cell Mol. Genet.* **13**, 279–284 (1987).
10. Abe, K. *et al.* Contribution of Asian mouse subspecies *Mus musculus molossinus* to genomic constitution of strain C57BL/6J, as defined by BAC-end sequence-SNP analysis. *Genome Res.* **14**, 2439–2447 (2004).
11. Itoh, T., Linn, S., Ono, T. & Yamaizumi, M. Reinvestigation of the classification of five cell strains of xeroderma pigmentosum group E with reclassification of three of them. *J. Invest. Dermatol.* **114**, 1022–1029 (2000).
12. Strausberg, R.L. *et al.* Generation and initial analysis of more than 15,000 full-length human and mouse cDNA sequences. *Proc. Natl. Acad. Sci. USA* **99**, 16899–16903 (2002).
13. Meinhart, A. & Cramer, P. Recognition of RNA polymerase II carboxy-terminal domain by 3′-RNA-processing factors. *Nature* **430**, 223–226 (2004).
14. Steinmetz, E.J., Conrad, N.K., Brow, D.A. & Corden, J.L. RNA-binding protein Nrd1 directs poly(A)-independent 3′-end formation of RNA polymerase II transcripts. *Nature* **413**, 327–331 (2001).
15. Khoronenkova, S.V., Dianova, I.I., Parsons, J.L. & Dianov, G.L. USP7/HAUSP stimulates repair of oxidative DNA lesions. *Nucleic Acids Res.* **39**, 2604–2609 (2011).
16. Schwertman, P. *et al.* UV-sensitive syndrome protein UVSSA recruits USP7 to regulate transcription-coupled repair. *Nat. Genet.* published online (1 April 2012); doi:10.1038/ng.2230.
17. Kamiuchi, S. *et al.* Translocation of Cockayne syndrome group A protein to the nuclear matrix: possible relevance to transcription-coupled DNA repair. *Proc. Natl. Acad. Sci. USA* **99**, 201–206 (2002).
18. Fousteri, M., Vermeulen, W., vanZeeland, A.A. & Mullenders, L.H. Cockayne syndrome A and B proteins differentially regulate recruitment of chromatin remodeling and repair factors to stalled RNA polymerase II *in vivo*. *Mol. Cell* **23**, 471–482 (2006).
19. Saijo, M. *et al.* Functional TFIIH is required for UV-induced translocation of CSA to the nuclear matrix. *Mol. Cell. Biol.* **27**, 2538–2547 (2007).
20. Rockx, D.A. *et al.* UV-induced inhibition of transcription involves repression of transcription initiation and phosphorylation of RNA polymerase II. *Proc. Natl. Acad. Sci. USA* **97**, 10503–10508 (2000).
21. Spivak, G. & Hanawalt, P.C. Host cell reactivation of plasmids containing oxidative DNA lesions is defective in Cockayne syndrome but normal in UV-sensitive syndrome fibroblasts. *DNA Repair (Amst.)* **5**, 13–22 (2006).
22. D'Errico, M. *et al.* The role of CSA in the response to oxidative DNA damage in human cells. *Oncogene* **26**, 4336–4343 (2007).
23. Selby, C.P. & Sancar, A. Cockayne syndrome group B protein enhances elongation by RNA polymerase II. *Proc. Natl. Acad. Sci. USA* **94**, 11205–11209 (1997).
24. Dianov, G.L., Houle, J.F., Iyer, N., Bohr, V.A. & Friedberg, E.C. Reduced RNA polymerase II transcription in extracts of cockayne syndrome and xeroderma pigmentosum/Cockayne syndrome cells. *Nucleic Acids Res.* **25**, 3636–3642 (1997).
25. Bradsher, J. *et al.* CSB is a component of RNA pol I transcription. *Mol. Cell* **10**, 819–829 (2002).
26. Lebedev, A., Scharffetter-Kochanek, K. & Iben, S. Truncated Cockayne syndrome B protein represses elongation by RNA polymerase I. *J. Mol. Biol.* **382**, 266–274 (2008).
27. Proietti-De-Santis, L., Drane, P. & Egly, J.M. Cockayne syndrome B protein regulates the transcriptional program after UV irradiation. *EMBO J.* **25**, 1915–1923 (2006).
28. Spivak, G. *et al.* Ultraviolet-sensitive syndrome cells are defective in transcription-coupled repair of cyclobutane pyrimidine dimers. *DNA Repair (Amst.)* **1**, 629–643 (2002).
29. Groisman, R. *et al.* CSA-dependent degradation of CSB by the ubiquitin-proteasome pathway establishes a link between complementation factors of the Cockayne syndrome. *Genes Dev.* **20**, 1429–1434 (2006).
30. Wei, L. *et al.* BRCA1 contributes to transcription-coupled repair of DNA damage through polyubiquitylation and degradation of Cockayne syndrome B protein. *Cancer Sci.* **102**, 1840–1847 (2011).
31. Takagi, Y. *et al.* Ubiquitin ligase activity of TFIIH and the transcriptional response to DNA damage. *Mol. Cell* **18**, 237–243 (2005).
32. Horibata, K. *et al.* Mutant Cockayne syndrome group B protein inhibits repair of DNA topoisomerase I–DNA covalent complex. *Genes Cells* **16**, 101–114 (2011).

ONLINE METHODS

Cell lines. Kps3, XP24KO and TA-24 cells belong to UV^{S}S-A and were immortalized by simian virus 40 large T antigen and hTERT. FS3 and WI38VA13 are normal human cells. Mouse A9 cells were used as donors in microcell-mediated chromosome transfer. All cell lines used were cultured in DMEM containing 10% FCS, penicillin and streptomycin at 37 °C under 5% CO_2.

UV survival. Cells were inoculated in 10-cm dishes at a density of 1,000–2,000 cells per dish. After 6 h, cells were washed with PBS and irradiated with UV at 0, 5 and 10 J/m^2. Cells were then incubated for 1–2 weeks. Resulting colonies were fixed with 3.7% formaldehyde and stained with 0.1% crystal violet and were counted using a binocular microscope.

Microcell-mediated chromosome transfer. Donor A9 cells were plated onto 25-cm^2 flasks in DMEM supplemented with 10% FCS. After 1–3 d (when cells were 80% confluent), the culture medium was changed to DMEM supplemented with 20% FCS and 50 ng/ml colcemid (Sigma). After 48 h of incubation, flasks were centrifuged at 12,000*g* for 1 h in the presence of 10 μg/ml cytochalasin B (Sigma) for enucleation. The microcell pellets were resuspended in serum-free DMEM and sequentially filtered through polycarbonate membranes with pores of 8, 5 and 3 μm in diameter. Purified microcells, which were irradiated with 10 Gy of γ-irradiation in some experiments, were plated onto a monolayer of recipient Kps3 cells in a 6-cm dish with serum-free DMEM containing 50 μg/ml phytohemagglutinin P (Sigma). After 30 min of incubation, the microcells were fused with recipient cells by treating the cells with 50% polyethylene glycol 1000 (Nakarai) for 1 min. After fusion, cells were grown for 24 h in DMEM supplemented with10% FCS. Then, cells were replated onto six 10-cm dishes and incubated for 24 h. Cells were irradiated with 10 J/m^2 of UV light. Surviving cells were collected and replated onto six 10-cm dishes and allowed to grow for 7 d. Cells were then irradiated with 10 J/m^2 of UV light. In total, cells were irradiated six times at 7-d intervals. As a negative control, Kps3 cells fused in the absence of microcells were UV irradiated in the same manner.

Comparative genomic hybridization array analysis. The regions of segmented mouse chromosomes transferred to Kps3 cells were analyzed using a Mouse Genome CGH 244A Oligo Microarray Kit with SurePrint Technology (Agilent Technologies), according to the manufacturer's instructions with some modifications. In brief, genomic DNA derived from the 15A-7, KAGB2-4, KAGA2-6 and KAB1-14 clones was compared with genomic DNA from parental Kps3 cells on the arrays. Genomic DNA was extracted by Qiagen Gentra Puregene core Kit A. After digestion with AluI and RsaI, the genomic DNA derived from Kps3 cells was labeled with Cy3, and the genomic DNA from the 15A-7, KAGB2-4, KAGA2-6 and KAB1-14 clones was labeled with Cy5, using a Genomic DNA Enzymatic Labeling Kit (Agilent Technologies). To prevent nonspecific hybridization of human genomic DNA on the array, 50 μg of human Cot-1 DNA (Invitrogen) and 5 μg of mouse Cot-1 DNA (Invitrogen) were mixed and subjected to prehybridization. After hybridization with the labeled genomic DNA, arrays were washed and scanned with GenePix4000B. Scanned data were analyzed by Feature Extraction Software version 9.5 and DNA Analytics version 4.0 (both from Agilent Technologies).

Transfection of mouse BACs. Mouse BAC clones were amplified in *Escherichia coli* cultured in LB medium containing chloramphenicol (25 μg/ml). BAC DNA was prepared with a Midiprep Kit (Qiagen), following the manufacturer's instructions. BAC DNA (20 μg) was cotransfected with 0.6 μg of pSV2neo into recipient Kps3 cells grown on a 10-cm tissue culture dish, and cells were selected with medium containing G418 (400 μg/ml) and irradiated with 10 J/m^2 of UV twice at 4–d intervals to examine whether the BAC-transfected Kps3 clones acquired a normal level of UV resistance.

Recovery of RNA synthesis after UV irradiation. To measure RNA synthesis after UV irradiation, two sets of cells were seeded into 6-well culture plates (1×10^6 cells/well). One set was used for counting cells and the other for measuring RNA synthesis. After 6 h of incubation, cells were washed with PBS and treated with UV at 10 J/m^2. After 2, 4, 8 and 24 h of incubation, the number of cells in one set was counted. The other set of cells was washed with PBS and incubated in DMEM containing 370 kBq/ml of [^{3}H]-uridine for 30 min to quantify RNA synthesis. Labeling was terminated by the addition of sodium azide to a final concentration of 200 μg/ml. Cells were washed twice with PBS containing 200 μg/ml sodium azide and lysed in 0.8% SDS for 30 min at room temperature. An equal volume of 10% trichloroacetic acid containing 0.1 M sodium pyrophosphate was then added to the lysates, and these were incubated on ice for 1 h. Acid-insoluble materials were collected on GF-C glass microfiber filters (Whatman), and radioactivity was measured with an LS 6500 liquid scintillation counter (Beckman Coulter). Total radioactivity was divided by the number of cells to obtain single-cell radioactivity. The ratio (as a percentage) of the radioactivity of individual UV-irradiated cells to that of non-irradiated cells was considered as a measure of the recovery of RNA synthesis after UV irradiation (UV-RRS).

Immunoprecipitation. Cells stably expressing a Flag- and HA-tagged protein were lysed with MNase buffer (20 mM Tris-HCl, pH 7.5, 100 mM KCl, 300 mM sucrose, 2 mM $MgCl_2$, 0.1% Triton X-100, 1 mM $CaCl_2$, 1 mM DTT and complete protease inhibitor cocktail (Roche)) at 4 °C for 10 min. Lysates were centrifuged at 3,800*g* for 5 min. Supernatant was used as the soluble fraction. The pellet was washed once with MNase buffer and incubated with 30 U/ml of micrococcal nuclease (Takara) in MNase buffer at 25 °C for 30 min. The reaction was terminated by adding EDTA to a 5 mM final concentration and centrifuged at 3,800*g* for 5 min at 4 °C. The pellet was washed with MNase buffer. Supernatants were combined and used as the solubilized chromatin fraction. Tagged protein was affinity purified from the soluble and solubilized chromatin fractions with anti-FLAG M2 antibody-conjugated agarose (Sigma) followed by anti-HA agarose (Sigma).

Knockdown experiments. siRNA (Thermo Scientific) was transfected into target cells with RNAiMAX (Invitrogen), according to the manufacturer's instructions. At 24 h after the first transfection, a second transfection was performed. Cells were allowed to grow for another 36 h before experiments were carried out.

Quantitative RT-PCR. cDNA was synthesized from fresh total RNA using a Quantitative Reverse Transcription kit (Qiagen), following the manufacturer's instructions. RT-PCR samples were prepared with TaqMan gene expression master mix (Applied Biosystems), according to the manufacturer's instructions. RT-PCR was carried out using the 7300 Real-Time PCR system (Applied Biosystems), under the following conditions: 10 s at 95 °C, 10 s at 60 °C and 20 s at 72 °C for 25 cycles. Probe sets were ordered from Applied Biosystems.

UV-induced translocation of ERCC8 to the nuclear matrix using a cell-free system. UV-induced translocation of ERCC8 in the cell-free system was examined as described previously[19]. Parental Kps3 cells and UVSSA-corrected Kps3 cells were irradiated with 20 J/m^2 of UV and incubated for 1 h and then treated with CSK-Triton buffer (10 mM PIPES, pH 6.8, 100 mM NaCl, 300 mM sucrose, 3 mM $MgCl_2$, 0.5% Triton X-100, 1 mM DTT, 1 mM EGTA and Complete protease inhibitor cocktail (Roche)) to prepare the insoluble (CSK-ppt) fractions. The soluble fractions (CSK-sup) were prepared from CS3BE (CS-A) cells stably expressing Flag- and HA-tagged ERCC8 by treatment with CSK-Triton buffer. The CSK-sup fraction containing HA-tagged ERCC8 was incubated with the CSK-ppt fraction and then treated with DNase I. The ERCC8 retained in the DNase I–insoluble fractions was detected by immunoblotting with antibody to HA.

Antibodies. The antibodies employed were to ERCC8 (W-16, Santa Cruz Biotechnology), ERCC6 (E-18, Santa Cruz Biotechnology), RNA Pol II (N-20 and A-10, Santa Cruz Biotechnology), KIAA1530 (106751, GeneTex) and HA (3F10, Roche).

Sato et al. BMC Musculoskeletal Disorders 2012, 13:51
http://www.biomedcentral.com/1471-2474/13/51

BMC Musculoskeletal Disorders

RESEARCH ARTICLE Open Access

Human telomerase reverse transcriptase and glucose-regulated protein 78 increase the life span of articular chondrocytes and their repair potential

Masato Sato[1*], Kazuo Shin-ya[2], Jeong Ik Lee[3], Miya Ishihara[4], Toshihiro Nagai[1], Nagatoshi Kaneshiro[1], Genya Mitani[1], Hidetoshi Tahara[5] and Joji Mochida[1]

Abstract

Background: Like all mammalian cells, normal adult chondrocytes have a limited replicative life span, which decreases with age. To facilitate the therapeutic use of chondrocytes from older donors, a method is needed to prolong their life span.

Methods: We transfected chondrocytes with hTERT or GRP78 and cultured them in a 3-dimensional atelocollagen honeycomb-shaped scaffold with a membrane seal. Then, we measured the amount of nuclear DNA and glycosaminoglycans (GAGs) and the expression level of type II collagen as markers of cell proliferation and extracellular matrix formation, respectively, in these cultures. In addition, we allografted this tissue-engineered cartilage into osteochondral defects in old rabbits to assess their repair activity in vivo.

Results: Our results showed different degrees of differentiation in terms of GAG content between chondrocytes from old and young rabbits. Chondrocytes that were cotransfected with hTERT and GRP78 showed higher cellular proliferation and expression of type II collagen than those of nontransfected chondrocytes, regardless of the age of the cartilage donor. In addition, the in vitro growth rates of hTERT- or GRP78-transfected chondrocytes were higher than those of nontransfected chondrocytes, regardless of donor age. In vivo, the tissue-engineered cartilage implants exhibited strong repairing activity, maintained a chondrocyte-specific phenotype, and produced extracellular matrix components.

Conclusions: Focal gene delivery to aged articular chondrocytes exhibited strong repairing activity and may be therapeutically useful for articular cartilage regeneration.

Background

Osteoarthritis (OA), which is one of the most common, debilitating, and costly chronic disorders [1], is characterized by progressive degeneration or destruction of articular cartilage. Since the incidence of OA increases with age, the underlying mechanism of this disease may involve a loss of the capacity of chondrocytes to regenerate with age. In proliferative cells, telomeres from chromosomes gradually became shorter as a result of the DNA replication end problem. To prevent cessation of mitosis and premature cell death, telomerase is a ribonucleoprotein that is an enzyme which adds DNA sequence repeats (TTAGGG) to the 3' end of DNA strands in the telomere regions, which are found at the ends of chromosomes [2]. The telomerase allows for replacement of short bits of DNA known as telomeres, which are otherwise shortened when a cell divides via mitosis. In normal circumstances, without the presence of telomerase, if a cell divides recursively, at some point all the progeny will reach their Hayflick limit. With the presence of telomerase, each dividing cell can replace the lost bit of DNA, and any single cell can then divide unbounded. While this unbounded growth property has excited many researchers, caution is warranted in exploiting this property, as exactly this same unbounded growth is a crucial step in enabling cancerous growth. In immortal human tumor cells, the gene for the catalytic subunit of

* Correspondence: sato-m@is.icc.u-tokai.ac.jp
[1]Department of Orthopaedic Surgery, Surgical Science, Tokai University School of Medicine, 143 Shimokasuya, Isehara, Kanagawa 259-1193, Japan
Full list of author information is available at the end of the article

human telomerase reverse transcriptase (*hTERT*) is almost always derepressed [3]. Moreover, *hTERT* is not only an oncoprotein [2] but also a regulator of cellular differentiation [4,5].

As a result, immortalized human cells, such as epithelial and fibroblast cells [6] and chondrocytes [7,8], have been used as models of cellular aging. For example, Goldring [7] showed that primary human chondrocytes can be immortalized with retroviral transfection of 4 genes, including simian vacuolating virus 40 large T antigen and telomerase; however, stable transfection of *hTERT* in chondrocytes that are cultured in a monolayer allows maintenance of the proliferative capacity but not the chondrocyte phenotype. In contrast, Piera-Velazquez et al. [8] showed that exogenous expression of *hTERT* in chondrocytes that are cultured on polyhydroxyethylmethacrylate coated dishes increases their life span and maintains their chondrocyte phenotype. Thus, *hTERT* may extend the life span of chondrocytes.

Glucose-regulated protein 78 (GRP78) is a molecular chaperone in the endoplasmic reticulum (ER) that is induced by ER stress and prevents cell death as a result of homeostatic imbalance in the ER [9]. Although overexpression of *GRP78* can limit the damage from ER stress in normal tissues and organs, the natural induction of GRP78 in neoplastic cells also may promote cancer progression and drug resistance [10]. Since *GRP78* also is involved in the pathology of neurological diseases, such as Alzheimer's disease [11] and Parkinson's disease [12], GRP78 may have therapeutic cytoprotective effects to limit ER stress.

To determine whether *hTERT* and *GRP78* can prolong the life span of chondrocytes and stimulate cartilage regeneration, we transfected rabbit articular chondrocytes with these genes and redifferentiated chondrocytes in a 3-dimensional atelocollagen honeycomb-shaped scaffold with a membrane seal (ACHMS scaffold) [13]. We used this type of scaffold because it is biodegradable, supports the growth of high-density cell cultures, and maintains the phenotype of articular chondrocytes [14-16]. In addition, to investigate the clinical relevance of our model to OA, we investigated whether the effects of gene transfection depend on the age of the cartilage by analyzing the proliferation, gross morphology, cellular content of DNA and proteoglycans, and gene expression level of type II collagen in the transfected chondrocytes.

Methods

Preparation of chondrocytes

All animal experiments in this study approved by Research Support and Intellectual Property of the University of Tokyo were performed in accordance with their institutional guidelines for the care and use of laboratory animals.

Chondrocytes were prepared as described previously [14]. Briefly, articular cartilage tissue specimens were collected from the knee and shoulder joints of 4 young male (4 weeks old, 1 kg) and 8 old female (4 years old, 4.5 kg) Japanese white rabbits (Tokyo Laboratory Animals Science Co., Ltd., Tokyo, Japan). Each rabbit specimen was soaked and stored separately in basal medium (BM) containing Dulbecco's modified Eagle's medium (DMEM)/F12 (Gibco; Invitrogen, Carlsbad, CA, USA) supplemented with 10% heat-inactivated fetal bovine serum (FBS) (Gibco), 50 $\mu g \cdot mL^{-1}$ ascorbic acid (Wako Pure Chemical Industries, Osaka, Japan), and 1% Fungizone® antibiotic-antimycotic solution (10,000 $U \cdot mL^{-1}$ penicillin G, 10 $mg \cdot mL^{-1}$ streptomycin sulfate, and 25 $\mu g \cdot mL^{-1}$ amphotericin B; Gibco). When needed, cartilage samples were chopped into small pieces, and then digested for 1 h in DMEM/F12 containing 0.4% pronase E (Kaken Pharmaceutical, Tokyo, Japan), followed by digestion for 3 h at 37°C in DMEM/F12 containing 0.016% collagenase P (Roche Diagnostics, Mannheim, Germany). Subsequently, the digested samples were filtered with a cell strainer (BD Falcon™; BD Bioscience, Bedford, MA, USA) with a 100 μm pore size and the isolated cells were rinsed twice with chilled Dulbecco's calcium- and magnesium-free, phosphate-buffered saline (PBS) (Dainippon Pharmaceutical, Osaka, Japan). The number of viable chondrocytes was counted by using a Burker-Turk hemocytometer (Erma, Tokyo, Japan) with Trypan blue staining. Finally, the chondrocytes were seeded in 500 cm^2 square dishes (245 mm × 245 mm; Corning, Corning, NY, USA) at a density of 10,000 $cells \cdot cm^{-2}$ and cultured in BM with 10% FBS at 37°C in an incubator with 5% CO_2.

Retroviral transfection

Retroviral transfection of cultured chondrocytes was performed as described previously [17,18] with some modifications. First, DH5α *Escherichia coli* cells (from Hiroshima University Graduate School of Biomedical Sciences) were cultured overnight in lysogeny broth (LB) media [19] at 37°C. Subsequently, these cells were transfected with p*hTERT*-MSCV and p*GRP78*-MSCV plasmids to produce amphotropic viruses. The plasmids were amplified and purified by using an EndoFree Plasmid Maxi Kit (Qiagen, Tokyo, Japan). In addition, the sequence of all constructs was verified by DNA sequencing.

Next, these plasmids were used to produce retroviral constructs by using 2 different protocols. To produce the *hTERT* retroviral construct, full-length *hTERT* cDNA was polymerase chain reaction (PCR) amplified, and then cloned into the pMSCV-puro retroviral vector (Clontech, Mountain View, CA, USA). Subsequently, the cloned vector was transfected into the Retropack PT67 (Clontech) packaging cell line and the transfected cells were selected with puromycin (1.8 $\mu g \cdot mL^{-1}$) (Sigma

Aldrich, St. Louis, MO, USA) after 48 h. Two weeks after transfection, the surviving cells were trypsinized and allowed to continue to grow for up to 100 d. The culture supernatant from this cell line was collected and 0.45-μm filtered, and then polybrene (8 $\mu g \cdot mL^{-1}$) was added prior to transducing *hTERT* into young rabbit (YRA) and old rabbit (ORA) chondrocyte cultures.

Chondrocytes were cultured and plated 24 h before viral infection. Then, the packaged retrovirus was added to the culture media and incubated at 37°C in an incubator with 5% CO_2. The infected cells were selected with 0.5 $\mu g \cdot mL^{-1}$ of puromycin (Sigma Chemical) for 7-10 d prior to subsequent experiments.

To produce the *GRP78* retroviral construct, full-length *GRP78* cDNA was PCR amplified, and then inserted into the mouse stem cell virus (MSCV) packaging vector by using the Retrovirus Packaging Kit Ampho (TaKaRa Biotechnology, Shiga City, Japan) [20]. To produce *GRP78*-expressing retroviruses, 293 T cells (CRL-11268™, ATCC, Manassas, VA, USA) were seeded and maintained on 6-cm dishes at a density of 400,000 $cells \cdot cm^{-2}$ in DMEM containing 10% FBS for 24 h prior to transfection. Then, the culture medium was changed to the same medium. Subsequently, the 293 T cells were co-transfected with pGP (gag-pol) and pE-ampho (env) (TaKaRa Biotechnology) by using calcium phosphate transfection. Transfected cells were selected with 400 $\mu g \cdot mL^{-1}$ of hygromycin (Calbiochem, La Jolla, CA, USA) and 50 μg of mycophenolic acid (Sigma Aldrich). After 48 h, the culture medium, which contained the recombinant retroviruses, was 0.45-μm filtered, and then mixed with DMEM to infect YRA and ORA chondrocyte cultures.

Chondrocyte proliferation

Chondrocyte proliferation was measured by counting cell numbers at 100% confluence in serial passages. Briefly, nontransfected or *hTERT/GRP78*-transfected YRA and ORA chondrocytes, which were passaged once every 7-10 d, were detached by using 0.05% trypsin/ethylenediaminetetraacetic acid (EDTA; Gibco) for 20-30 min at 37°C and washed 3 times with PBS. An aliquot of the detached cells was used to count the mean number of cells from 6 dishes by using a Burker-Turk hemocytometer (Erma) with Trypan blue staining. The remaining cells were replated at a density of 5×10^3 $cells \cdot well^{-1}$.

Cell proliferation was expressed as the population doubling level (PDL). The PDL was calculated from log-phase growth curves by using the equation: $PDL = \log_{10}(N/N_0) \times 3.33$, where N_0 and N are the number of cells at the beginning and end of each experiment, respectively [21].

Preparation of the atelocollagen honeycomb-shaped scaffold with a membrane seal and 3-dimensional culture of chondrocytes

The ACHMS scaffold was prepared as described previously [13] by Koken (Tokyo, Japan). Briefly, nontransfected and *hTERT/GRP78*-transfected ORA chondrocytes were passaged twice, and then seeded at a density of 2×10^6 $cells \cdot scaffold^{-1}$ into a round ACHMS scaffold (diameter, 6 mm; thickness, 2 mm; average pore size, 200 μm) [13,14,22,23] in 48-well plates (Sumitomo Bakelite, Tokyo, Japan) by centrifuging at 45 *g* for 5 min. Then, these cell-seeded scaffolds were cultured in BM supplemented with 10% FBS at 37°C in an incubator with 5% CO_2 and 100% relative humidity for 14 d. These cultured chondrocytes were frozen in liquid nitrogen until needed for biochemical analyses and transplantation into an in vivo model of articular cartilage defects.

Measurement of DNA and glycosaminoglycans

The amount of DNA in the cultured ORA chondrocytes, which was used as a marker of cell proliferation, was measured by digesting cell-seeded scaffolds with papain, and then using a fluorimetric assay, as described previously [24]. Briefly, 15 μL of a papain digest was mixed with 300 μL of Hoechst 33258 solution (Polyscience, Warrington, PA, USA), and then a Titertek Multiscan Spectrofluorometer (Lab Systems, Helsinki, Finland) was used to measure the emission and excitation spectra at 456 nm and 365 nm, respectively. DNA concentrations were calculated from a standard curve of calf thymus DNA (Sigma).

The amount of glycosaminoglycans (GAGs) in the cultured chondrocytes, which was used as a marker of extracellular matrix (ECM) formation, was quantified by using 1,9-dimethylmethylene blue, as described previously [25]. Briefly, samples (140 μL) of each chondrocyte culture were mixed gently with an equal volume of 1,9-dimethylmethylene blue solution in a 96-well microtiter plate, and then the absorbance at 530 nm was measured with a Titertec multiscan spectrophotometer (Labsystem, Helsinki, Finland). The amount of GAGs was calculated from the absorbance values by using a standard curve of 0.625-20 $\mu g \cdot mL^{-1}$ shark chondroitin sulfate C (Seikagaku Kogyo Co, Tokyo, Japan).

Type II collagen mRNA expression

Frozen 3-dimensional cultures of ORA chondrocytes were pulverized with a Cryo-Press (Microtec Nition, Chiba, Japan) in liquid nitrogen. All oligonucleotide primer sets were designed on the basis of published mRNA sequences. The expected amplicon lengths ranged from 70 to 200 bp. Cloning of the entire coding region of type 2 collagen was performed by 5'- and 3'-rapid amplification of cDNA ends

using the following oligonucleotide primers: forward (5'-AACACTGCCAACGTCCAGAT-3'), reverse (5'-CTGC AGCACGGTATAGGTGA-3'). Real-time PCR was performed in a SmartCycler system (Cepheid, Sunnyvale, CA) with SYBR Green PCR Master Mix (Applied Biosystems, Foster City, CA) with 1 μL of cDNA template in a final volume of 25 μL. Amplification of cDNA was performed according to the following conditions: 95°C for 15 s and 60°C for 60 s for 35-45 amplification cycles. Changes in the fluorescence of SYBR Green were monitored after every cycle. Melting curve analysis was performed through a 0.5°C/s increase from 55 to 95°C with continuous fluorescence readings at the end of the cycles to ensure that single PCR products were obtained. All reactions were repeated in six separate PCR runs using RNA isolated from four sets of human samples. The results were evaluated by using SmartCycler software (Cepheid). Glyceraldehyde-3-phosphate dehydrogenase (GAPDH) primers were used to normalize the samples. To monitor crossover contaminations of PCR, RNase-free water (Qiagen, Valencia, CA) was used in the RNA extraction and as a negative control. To ensure the quality of data, a negative control was always included in each run.

Implantation of tissue-engineered cartilage produced from transfected aged chondrocytes

Twenty four old female Japanese white rabbits were divided into 4 groups (control 8w, 16w; hTERT + GRP78 8w, 16w) and anesthetized with intramuscular injections of 120 mg of ketamine (Daiichisankyo, Tokyo, Japan) and 9 mg of xylazine (Bayer HealthCare, Leverkusen, Germany). After creating a medial parapatellar incision in both legs, each patella was dislocated laterally and a cylindrical defect (diameter, 5 mm; depth, 3 mm) was created on the patellar groove of the femur in both legs by using a biopsy punch (Kai Industries, Seki, Japan) and a low-speed drill (Takagi, Niigata, Japan). The bottom of the subchondral bone also was shaved to a plane until marrow bleeding was observed. Then, ACHMS scaffolds that were seeded with either nontransfected or *hTERT*/*GRP78*-transfected ORA chondrocytes were allografted into these defects without any fixatives, such as fibrin glue. Postoperatively, all animals were allowed to walk freely in their cages without any splints.

Postoperative analyses

Eight and 16 weeks after implantation, rabbits were killed with an overdose of intravenous anesthesia, and then the distal parts of their femurs were harvested and observed with a light microscope. Subsequently, the femur samples were fixed in 10% buffered formalin for 7 d. Each specimen was decalcified with 10% EDTA in distilled water (pH 7.4) for 3 weeks, and then embedded in paraffin, cut into 6-μm-thick sagittal sections, deparaffinized, and stained with safranin O (Cartilage Staining Kit, Takara, Shiga, Japan). The histopathology of the OA cartilage samples (n = 24) were analyzed according to standard grading and staging of OA cartilage histopathology [26]. The OA score was calculated by the following formula: OA score = most degenerated site in the cartilage (grades 1-6, Table 1) × area of degeneration (stages 1-4) (Table 2).

Immunohistochemical staining for type II collagen was performed as described previously [14]. Briefly, after deparaffinization, the sections were pretreated with 0.1 $mg{\cdot}mL^{-1}$ of actinase E (Kaken Pharmaceutical) in PBS at 37°C for 30 min. Then, the sections were incubated with 10% pig serum at room temperature for 30 min to reduce nonspecific background staining. These pretreated sections were incubated overnight with 50 $mg{\cdot}mL^{-1}$ mouse anti-human type II collagen monoclonal antibody (Daiichi Fine Chemical, Toyama, Japan) in PBS containing 0.1% bovine serum albumin at 4°C. Next, the sections were incubated with biotinylated rabbit anti-mouse immunoglobulin (1:500 dilution; Dako, Carpinteria, CA, USA) for 30 min at room temperature, followed by peroxidase-conjugated streptavidin (1:500 dilution; Dako) for 30 min at room temperature. Finally, the sections were incubated with a solution of 20 mg of diaminobenzidine and 5 μL of hydrogen peroxide (30%) in 100 mL of PBS for 5 min at room temperature. Control sections were incubated with PBS without any antibodies and stained in a similar manner. These sections were analyzed by light microscopy.

Statistical analysis

One-way analysis of variance and Dunn's post hoc test was used to determine statistical significance ($P < 0.05$).

Results

Establishment of primary cultures of rabbit chondrocytes

During the first 3 weeks, YRA, ORA, ORA + *hTERT*, and ORA + *hTERT* + *GRP78* chondrocytes showed similar growth rates for 10 PDL (Figure 1). Later, ORA + *hTERT* and ORA + *hTERT* + *GRP78* chondrocytes proliferated more rapidly than the nontransfected chondrocytes. However, YRA + *hTERT* + *GRP78* chondrocytes had the fastest growth rate. In the control groups, YRA chondrocytes proliferated faster than ORA chondrocytes during the entire observation period, but their growth rate gradually decreased until they ceased at about 40 d and 60 d after the initiation of culture, respectively. Unlike control cells, which stopped proliferating after 10-20 PDL, ORA + *hTERT* and YRA + *hTERT* cells continued proliferating for about 35 and 50 PDL, respectively. These results showed that *hTERT* and *GRP78* increase the growth rate of transfected cells approximately 3-fold compared with nontransfected cells.

Table 1 OA cartilage histopathology grade assessment; grading methodology

Grade (key feature)	Associated criteria (tissue reaction)
Grade 1: surface intact	Matrix: superficial zone intact, oedema and/or superficial fibrillation (abrasion), focal superficial matrix condensation Cells: death, proliferation (clusters), hypertrophy, superficial zone Reaction must be more than superficial fibrillation only
Grade 2: surface discontinuity	As above + Matrix discontinuity at superficial zone (deep fibrillation) ± Cationic stain matrix depletion (Safranin O or Toluidine Blue) upper 1/3 of cartilage ± Focal perichondronal increased stain (mid zone) ± Disorientation of chondron columns Cells: death, proliferation (clusters), hypertrophy
Grade 3: vertical fissures (clefts)	As above Matrix vertical fissures into mid zone, branched fissures ± Cationic stain depletion (Safranin O or Toluidine Blue) into lower 2/3 of cartilage (deep zone) ± New collagen formation (polarized light microscopy, Picro Sirius Red stain) Cells: death, regeneration (clusters), hypertrophy, cartilage domains adjacent to fissures
Grade 4: erosion	Cartilage matrix loss: delamination of superficial layer, mid layer cyst formation Excavation: matrix loss superficial layer and mid zone
Grade 5: denudation	Surface: sclerotic bone or reparative tissue including fibrocartilage within denuded surface. Microfracture with repair limited to bone surface
Grade 6: deformation	Bone remodelling (more than osteophyte formation only). Includes: microfracturewith fibrocartilaginous and osseous repair extending above the previous surface

Grade = depth progression into cartilage

Characteristics of the 3-dimensional cultures of chondrocytes

The ACHMS scaffold supported a high density of ORA chondrocytes (2×10^6 cells·cm^{-2}) without any leakage of cells. During the 2-week culture, the chondrocytes in the scaffold retained their normal spherical shape (data not shown) and the resulting tissue-engineered cartilage maintained its shape and size in the ACHMS scaffold. The scaffolds were elastic and did not deform during culturing or collapse when handled with forceps.

Figure 2 shows macroscopic images of the cell-seeded scaffolds after culturing for 14 d. The scaffold that was seeded with *hTERT/GRP78*-transfected ORA chondrocytes had the highest cell density. In addition, the spaces between the atelocollagen matrix were filled and not visible along the edge of the ACHMS scaffold, which indicated that chondrocytes had proliferated throughout the scaffold during the cultivation period. In the scaffolds that were seeded with control cells, cell growth was sparse, and as a result, the spaces between the atelocollagen matrix remained mostly empty.

Glycosaminoglycan content of cell-seeded scaffolds

On day 14, the amount of GAG in cell-seeded scaffolds differed significantly between each group (Figure 3). Specifically, the total GAG content of scaffolds that were seeded with *hTERT/GRP78*-transfected ORA chondrocytes was higher than those that were seeded with *GRP78*- or *hTERT*-transfected cells. In addition, the GAG content of the scaffolds that were seeded with transfected ORA chondrocytes was higher than that in those that were seeded with nontransfected chondrocytes. These results suggested that transfected ORA chondrocytes were able to produce and accumulate significantly higher amounts of extracellular matrix components in the ACHMS scaffold than nontransfected chondrocytes.

Table 2 OA score; semi-quantitative method

Grade (key feature)	Stage % Involvement (surface, area, volume)			
	Stage 1 < 10%	Stage 2 10-25%	Stage 3 25-50%	Stage 4 > 50%
Grade 1(surface intact)	1	2	3	4
Grade 2 (surface discontinuity)	2	4	6	8
Grade 3 (vertical fissures, clefts)	3	6	9	12
Grade 4 (erosion)	4	8	12	16
Grade 5(denudation)	5	10	15	20
Grade 6(deformation)	6	12	18	24

Score = grade × stage

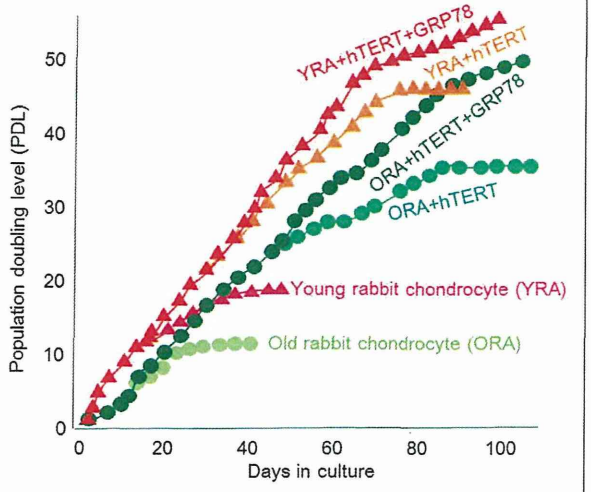

Figure 1 Effect of *hTERT* and *GRP78* on the proliferation of rabbit chondrocytes. Growth curves of cultures of nontransfected control chondrocytes from young and old rabbits (YRA and ORA, respectively) and *hTERT* (YRA + *hTERT* and ORA + *hTERT*) and *GRP78* (YRA + *hTERT* + *GRP78* and ORA + *hTERT* + *GRP78*)-transfected chondrocytes. The mean number of cells is shown on a $\log_{10}$ scale.

Type II collagen mRNA expression

As shown in Figure 4, the mRNA expression of type II collagen was observed in ORA, regardless of different gene transfection. Profiles of control, *GRP78*$^+$, *hTERT*$^+$, and *hTERT*$^+$/*GRP78*$^+$ cells were prepared to investigate expression of type II collagen. The mRNA expressions of *GRP78*$^+$, *hTERT*$^+$, and *hTERT*$^+$/*GRP78*$^+$ cells were significantly higher than that in control of non-transfective ORA. Chondrocytes are known to readily dedifferenciate in 2-dimensional culture. However, in this study, we used the primary culture of chondrocytes so that these chondrocytes retain their phenotype, which can be confirmed from type II collagen expression.

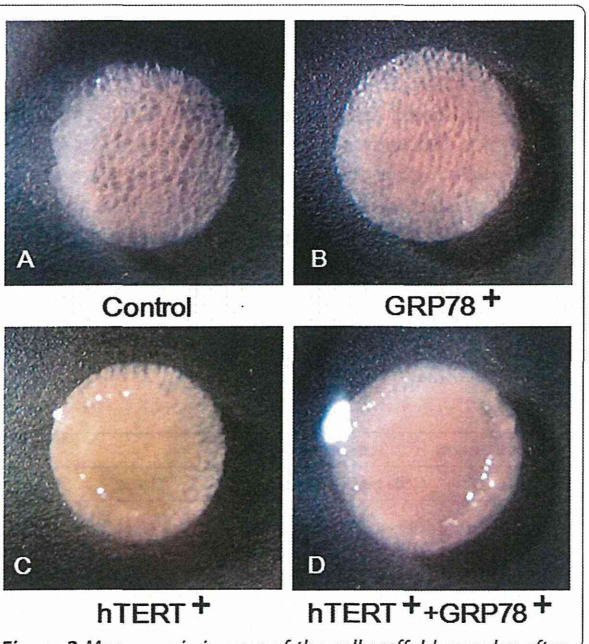

Figure 2 Macroscopic images of the cell-scaffold complex after 14 days of culture. Atelocollagen honeycomb-shaped scaffold with a membrane seal (ACHMS) scaffold complex seeded with nontransfected (A), *GRP78*-transfected (B), *hTERT*-transfected (C), or *hTERT*- and *GRP78*-transfected (D) ORA chondrocytes. Scale bar = 1.0 mm.

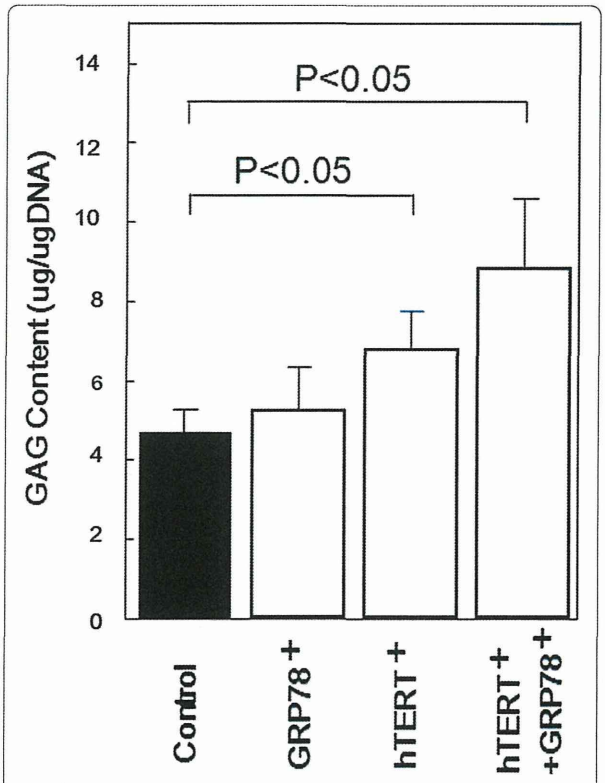

Figure 3 Glycosaminoglycan content of chondrocyte cultures in atelocollagen honeycomb-shaped scaffolds with a membrane seal. The glycosaminoglycan (GAG) content of nontransfected (black bars) or *hTERT*- or *GRP78*-transfected (white bars) ORA chondrocytes on the indicated days. Results are expressed as the mean (SD) of 6 independent measurements. *$P < 0.05$.

Macroscopic appearance of repaired osteochondral defects

The surgical implantation of tissue-engineered cartilage into osteochondral defects in the old rabbits was uneventful, and upon waking, all rabbits immediately resumed normal cage activity. At the time that they were killed, all rabbits exhibited unlimited passive range of motion in the knee joint.

Indeed, the osteochondral defects in old rabbits that were treated with tissue-engineered cartilage that was

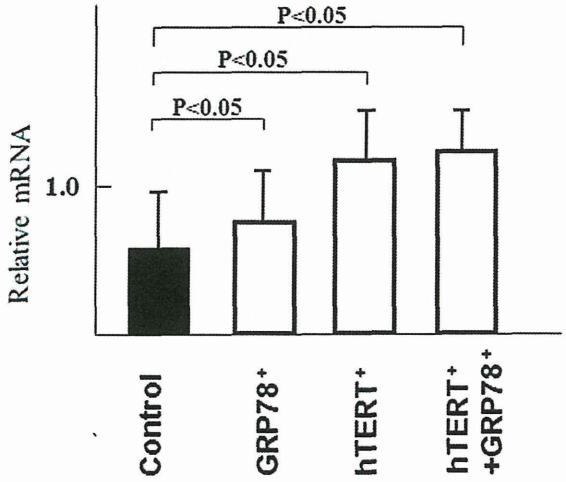

Figure 4 mRNA expression levels of type II collagen in transfected chondrocytes. The mRNA expression of type II collagen was observed in ORA, regardless of different gene transfection. Profiles of control, *GRP78*$^+$, *hTERT*$^+$, and *hTERT*$^+$/*GRP78*$^+$ cells were prepared to investigate expression of type II collagen. The mRNA expressions of *GRP78*$^+$, *hTERT*$^+$, and *hTERT*$^+$/*GRP78*$^+$ cells were significantly higher than that in control of non-transfective ORA. GAPDH was used as an internal control to normalize RNA levels.

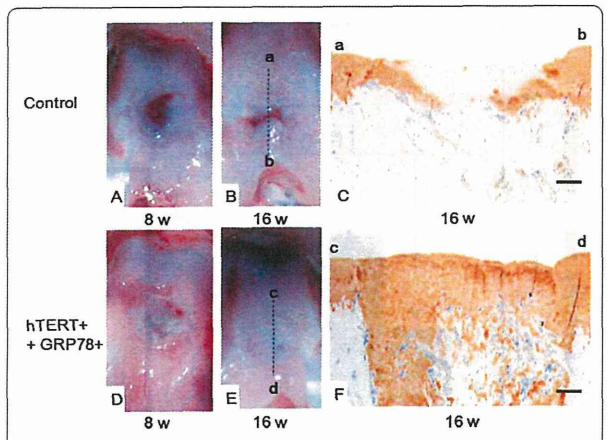

Figure 5 Macroscopic and immunostaining of regenerated cartilage after implantation. Postoperative appearance of repaired osteochondral defects in old rabbits implanted with scaffolds seeded with either nontransfected (top panels) or *hTERT*- and *GRP78*-transfected ORA chondrocytes (bottom panels) either 8 (A, D) or 16 (B, E) weeks after surgery. Immunostaining of type II collagen in tissue sections from rabbits implanted with scaffolds seeded with nontransfected (C) or *hTERT*- and *GRP78*-transfected (F) ORA chondrocytes. Each micrograph is representative of 8 tissue samples. Scale bar = 1.0 mm.

grown from *hTERT*- and *GRP78*-transfected ORA chondrocytes were filled with smooth tissue that resembled hyaline cartilage 16 weeks after surgery (Figure 5E) unlike the tissue-engineered cartilage that was grown from nontransfected ORA chondrocytes, which remained empty or were covered by fibrous tissue (Figure 5B). Although the control tissue-engineered cartilage showed some tissue repair along the borders of the defect, the color of the tissue was slightly different from that of the surrounding normal cartilage (Figure 5A, B).

Histological analysis of repaired osteochondral defects

No signs of arthritis, such as cartilage erosion or severe synovial proliferation, were observed in any surgically treated knee. In rabbits that were implanted with tissue-engineered cartilage grown from *hTERT*- and *GRP78*-transfected ORA chondrocytes, the immunohistochemical staining for type II collagen in the extracellular matrix in the scaffold was more intense and covered a larger area (Figure 5F) than those that were implanted with scaffolds that were grown from nontransfected ORA chondrocytes (Figure 5C). In addition, the tissue-engineered cartilage that was grown from transfected ORA chondrocytes was smooth and displayed good bonding with the host cartilage on both sides. In contrast, the tissue-engineered cartilage that was grown from nontransfected ORA chondrocytes had an irregular surface and was thinner than that grown from *hTERT*- and *GRP78*-transfected chondrocytes (Figure 5C).

As shown in Figure 6, the average OA scores were as follows: control 8w, 11.2 (2.5); 16w, 16.0 (3.2); hTERT + GRP78 8w, 17.3 (3.5); 16w, 21.00 (2.85). Statistically significant differences ($P < 0.05$) were observed between the transfected and nontransfected groups that were observed for the same period of time after implantation.

Discussion

Aging is the most important risk factor for both the initiation and progression of degenerative cartilage diseases. Osteoarthritic cartilage degeneration may be due to the loss of viable chondrocytes due to apoptosis or physical stress. This degeneration is likely to be closely related to age-related changes, since aging chondrocytes and articular cartilage matrix undergo senescence-like changes, which increase the susceptibility of cells to degenerative processes and environmental or physiological stresses [27]. As a result, chondrocytes from osteoarthritic patients might progress toward senescence more rapidly than those from normal individuals.

Aging chondrocytes also have important therapeutic ramifications. Recently, the treatment of articular cartilage defects have improved with the introduction of advanced tissue engineering techniques for autologous chondrocyte implantation (ACI) [28]. ACI requires cell expansion in culture to provide sufficient amounts of chondrocytes for reimplantation. However, like all mammalian cells, normal adult chondrocytes have a limited mitotic potential and eventually enter a state of senescence [29]. Moreover, the

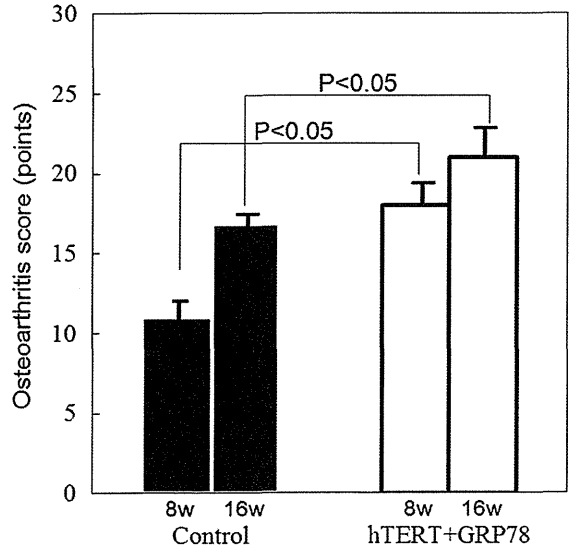

Figure 6 Osteoarthritis score. The histopathology of the OA cartilage samples from all 4 groups (n = 24) were analyzed according to standard grading and staging of OA cartilage histopathology. OA scores were calculated by using the following formula: OA score = most degenerated site in the cartilage (grades 1-6, Table 1) × area of degeneration (stages 1-4) (Table 2). Error bars indicate the standard deviation of each group. Statistically significant differences were observed between the control and hTERT + GRP78 groups 8 and 16 weeks after transplantation.

replicative life span of primary cells in culture are affected by the age of the donor, such that cells from older donors have a shorter life spans than those from younger donors [30]. For example, in monolayer cultures of aged human chondrocytes, serial passages rapidly results in loss of phenotypic stability and proliferative capacity [7]. Thus, to facilitate the therapeutic use of chondrocytes from older donors, a method is needed to prolong their replicative life span.

One possible method is transfection of *hTERT*, which can immortalize or prolong the life span of various human cells, such as muscle satellite cells [31,32], myoblasts [33,34], fibroblasts [6], and chondrocytes [7,8]. Since most immortalized cells maintain their phenotype and state of differentiation, *hTERT*-transfected cells are considered potential therapies for small-cell lung cancer [35] and for postnatal neovascularization in severe ischemic disease [36]. However, since chondrocytes uniquely maintain their phenotypes in 3-dimensional cultures [37], it is not known whether *hTERT*-immortalized chondrocytes maintain their state of differentiation.

Due to the aforementioned issues, in most cartilage tissue engineering studies, donor chondrocytes are usually from young animals. Our study is the first report that transfection of *hTERT* and *GRP78* can increase the replicative life span and therapeutic potential of tissue-engineered cartilage that is produced from ORA chondrocytes, which have a limited regenerative capacity. In addition, we used an ACHMS scaffold to maintain the phenotype of transfected chondrocytes, as indicated by the production of GAGs and type II collagen (Figures 3 and 4). These results are consistent with the findings of Piera-Velazquez et al. [8].

In this study, we overcame the limited lifespan of ORA chondrocytes by transfection with *hTERT* and increased their growth rate up to 3-fold by cotransfection with *GRP78* (Figure 1). Specifically, *hTERT/GRP78*-transfected ORA chondrocytes grew at a constant rate for more than 20 PDL, whereas nontransfected chondrocytes stopped dividing after much fewer PDL. However, we were not able to completely immortalize chondrocytes, even those from young rabbits (PDL < 50). Although the additional transfection of SV40-TAg or mutant Ras could immortalize these cells, we did not choose this option because the transfected cells may have become cancerous. As a result, we focused on the phenotypic stability of GRP78 and hTERT.

hTERT is a candidate gene for gene therapy of muscular dystrophy [31-34]. In contrast, *GRP78* may have therapeutic applications for neuropathological conditions, such as Alzheimer's disease, because it protects cells from ER stress [11,38-40]. ER stress can alter protein synthesis in cells [41]. One mechanism by which ER stress promotes apoptosis in cells is by driving the accumulation of structurally abnormal proteins [42], which are ordinarily repaired by ER chaperones to prevent age-related cell death. GRP78 is an example of a chaperone protein that regulates protein folding in the ER and thus contributes to cell survival [43]. Since the increase in the expression of GRP78 during cell culture may help protect cells from ER stress, overexpression of GRP78 also may protect cultured chondrocytes independent of hTERT.

Due to a lack of cages for mutant rabbits, we were not able to perform animal transplantation experiments with chondrocytes that were transfected with *hTERT* or *GRP78* alone. However, we believe that our in vitro and in vivo results from chondrocytes that were transfected with both *hTERT* and *GRP78* are sufficient to support our conclusions. In the future, we plan to perform more animal experiments to elucidate the effects of *GRP78*.

In conclusion, our results showed that tissue-engineered cartilage that was grown from implanted *in vivo* with *hTERT*- and *GRP78*-transfected ORA chondrocytes in ACHMS scaffolds can repair articular cartilage defects in vivo (Figure 5D, E, F). The *hTERT* and *GRP78*-transfected ORA exhibited proliferative and differentiation activity in articular cartilage defects, resulting in the formation of hyaline cartilage. This study also shows that ORA chondrocytes potentially produce hyaline cartilage after genetic treatment, similar to chondrocytes from young animals.

However, the mechanical strength of regenerated articular cartilage in large animals (*i.e.*, sheep or pigs) needs to be investigated.

Abbreviations

hTERT: Human telomerase reverse transcriptase; GRP78: Glucose-regulated protein 78; ER: Endoplasmic reticulum; ACHMS scaffold: Atelocollagen honeycomb-shaped scaffold with a membrane seal; OA: Osteoarthritis; BM: Basal medium; DMEM: Dulbecco's modified Eagle's medium; FBS: Fetal bovine serum; YRA: Young rabbit; ORA: Old rabbit; PDL: Population doubling level; RT-PCR: Reverse transcriptase-polymerase chain reaction; GAPDH: Gylceraldehyde-3-phosphate dehydrogenase; ACI: Autologous chondrocyte implantation; ECM: Extracellular matrix.

Acknowledgements

This work was supported by the Takeda Science Foundation, Grant of the New Energy and Industrial Technology Development Organization, and High-Tech Research Center Project 2004 for Private University. The funders had no role in study design, data collection and analysis, decision to publish, or preparation of the manuscript.

Author details

[1]Department of Orthopaedic Surgery, Surgical Science, Tokai University School of Medicine, 143 Shimokasuya, Isehara, Kanagawa 259-1193, Japan. [2]Biomedicinal Information Research Center, National Institute of Advanced Industrial Science and Technology (AIST), 2-42 Aomi, Koto-ku, Tokyo 135-0064, Japan. [3]Department of Biomedical Science & Technology, Institute of Biomedical Science & Technology (IBST), Konkuk University, 1 Hwang-dong, Gwangjin-gu, Seoul 143-701, Korea. [4]Department of Medical Engineering, National Defense Medical College, 3-2 Namiki, Tokorozawa, Saitama 359-8513, Japan. [5]Hiroshima University Graduate School of Biomedical Sciences, 1-2-3 Kasumi, Minami-ku, Hiroshima 734-8553, Japan.

Authors' contributions

MS, KS, MI, and TN conducted the experiments. MS, MI, NK, TK, HT, and GM analyzed the data. JIL performed the statistical analyses. MS, JIL, and JM wrote the manuscript. All authors read and approved the final manuscript.

Competing interests

The authors declare that they have no competing interests.

Received: 3 November 2011 Accepted: 2 April 2012
Published: 2 April 2012

References

1. Issa SN, Sharma L: **Epidemiology of osteoarthritis: an update.** *Curr Rheumatol Rep* 2006, **8**:7-15.
2. Harley CB: **Telomerase is not an oncogene.** *Oncogene* 2002, **21**:494-502.
3. Meyerson M, Counter CM, Eaton EN, Ellisen LW, Steiner P, Caddle SD, Ziaugra L, Beijersbergen RL, Davidoff MJ, Liu Q, Bacchetti S, Haber DA, Weinberg RA: **hEST2, the putative human telomerase catalytic subunit gene, is up-regulated in tumor cells and during immortalization.** *Cell* 1997, **90**:785-795.
4. Mattson MP, Fu W, Zhang P: **Emerging roles for telomerase in regulating cell differentiation and survival: a neuroscientist's perspective.** *Mech Ageing Dev* 2001, **122**:659-671.
5. Liu L, DiGirolamo CM, Navarro PA, Blasco MA, Keefe DL: **Telomerase deficiency impairs differentiation of mesenchymal stem cells.** *Exp Cell Res* 2004, **294**:1-8.
6. Hahn WC, Counter CM, Lundberg AS, Beijersbergen RL, Brooks MW, Weinberg RA: **Creation of human tumour cells with defined genetic elements.** *Nature* 1999, **400**:464-468.
7. Goldring MB: **Immortalization of human articular chondrocytes for generation of stable, differentiated cell lines.** *Methods Mol Med* 2004, **100**:23-36.
8. Piera-Velazquez S, Jimenez SA, Stokes D: **Increased life span of human osteoarthritic chondrocytes by exogenous expression of telomerase.** *Arthritis Rheum* 2002, **46**:683-693.
9. Reddy RK, Mao C, Baumeister P, Austin RC, Kaufman RJ, Lee AS: **Endoplasmic reticulum chaperone protein GRP78 protects cells from apoptosis induced by topoisomerase inhibitors: role of ATP binding site in suppression of caspase-7 activation.** *J Biol Chem* 2003, **278**:20915-20924.
10. Lee AS: **The glucose-regulated proteins: stress induction and clinical applications.** *Trends Biochem Sci* 2001, **26**:504-510.
11. Katayama T, Imaizumi K, Manabe T, Hitomi J, Kudo T, Tohyama M: **Induction of neuronal death by ER stress in Alzheimer's disease.** *J Chem Neuroanat* 2004, **28**:67-78.
12. Ryu EJ, Harding HP, Angelastro JM, Vitolo OV, Ron D, Greene LA: **Endoplasmic reticulum stress and the unfolded protein response in cellular models of Parkinson's disease.** *J Neurosci* 2002, **22**:10690-10698.
13. Sato M, Asazuma T, Ishihara M, Kikuchi T, Masuoka K, Ichimura S, Kikuchi M, Kurita A, Fujikawa K: **An atelocollagen honeycomb-shaped scaffold with a membrane seal (ACHMS-scaffold) for the culture of annulus fibrosus cells from an intervertebral disc.** *J Biomed Mater Res A* 2003, **64**:248-256.
14. Masuoka K, Asazuma T, Ishihara M, Sato M, Hattori H, Ishihara M, Yoshihara Y, Matsui T, Takase B, Kikuchi M, Nemoto K: **Tissue engineering of articular cartilage using an allograft of cultured chondrocytes in a membrane-sealed atelocollagen honeycomb-shaped scaffold (ACHMS scaffold).** *J Biomed Mater Res B Appl Biomater* 2005, **75**:177-184.
15. Ishihara M, Sato M, Sato S, Kikuchi T, Mochida J, Kikuchi M: **Usefulness of photoacoustic measurements for evaluation of biomechanical properties of tissue-engineered cartilage.** *Tissue Eng* 2005, **11**:1234-1243.
16. Glowacki J, Mizuno S: **Collagen scaffolds for tissue engineering.** *Biopolymers* 2008, **89**:338-344.
17. Pear WS, Nolan GP, Scott ML, Baltimore D: **Production of high-titer helper-free retroviruses by transient transfection.** *Proc Natl Acad Sci USA* 1993, **90**:8392-8396.
18. Fujita T, Otsuka-Tanaka Y, Tahara H, Ide T, Abiko Y, Mega J: **Establishment of immortalized clonal cells derived from periodontal ligament cells by induction of the hTERT gene.** *J Oral Sci* 2005, **47**:177-184.
19. Bertani G: **Lysogeny at mid-twentieth century: P1, P2, and other experimental systems.** *J Bacteriol* 2004, **186**:595-600.
20. Hawley RG, Lieu FH, Fong AZ, Hawley TS: **Versatile retroviral vectors for potential use in gene therapy.** *Gene Ther* 1994, **1**:136-138.
21. Cristofalo VJ, Allen RG, Pignolo RJ, Martin BG, Beck JC: **Relationship between donor age and the replicative lifespan of human cells in culture: a reevaluation.** *Proc Natl Acad Sci USA* 1998, **95**:10614-10619.
22. Itoh H, Aso Y, Furuse M, Noishiki Y, Miyata T: **A honeycomb collagen carrier for cell culture as a tissue engineering scaffold.** *Artif Organs* 2001, **25**:213-217.
23. Hattori H, Sato M, Masuoka K, Ishihara M, Kikuchi T, Matsui T, Takase B, Ishizuka T, Kikuchi M, Fujikawa K, Ishihara M: **Osteogenic potential of human adipose tissue-derived stromal cells as an alternative stem cell source.** *Cells Tissues Organs* 2004, **178**:2-12.
24. Kim YJ, Sah RL, Doong JY, Grodzinsky AJ: **Fluorometric assay of DNA in cartilage explants using Hoechst 33258.** *Anal Biochem* 1988, **174**:168-176.
25. Farndale RW, Buttle DJ, Barrett AJ: **Improved quantitation and discrimination of sulphated glycosaminoglycans by use of dimethylmethylene blue.** *Biochim Biophys Acta* 1986, **883**:173-177.
26. Pritzker KP, Gay S, Jimenez SA, Ostergaard K, Pelletier JP, Revell PA, Salter D, van den Berg WB: **Osteoarthritis cartilage histopathology: grading and staging.** *Osteoarthritis Cartilage* 2006, **14**:13-29.
27. Aigner T, Rose J, Martin J, Buckwalter J: **Aging theories of primary osteoarthritis: from epidemiology to molecular biology.** *Rejuvenation Res* 2004, **7**:134-145.
28. Brittberg M, Lindahl A, Nilsson A, Ohlsson C, Isaksson O, Peterson L: **Treatment of Deep Cartilage Defects in the Knee with Autologous Chondrocyte Transplantation.** *N Engl J Med* 1994, **331**:889-895.
29. Evans CH, Georgescu HI: **Observations on the senescence of cells derived from articular cartilage.** *Mech Ageing Dev* 1983, **22**:179-191.
30. Hayflick L: **The limited in vitro lifetime of human diploid cell strains.** *Exp Cell Res* 1965, **37**:614-636.
31. Cudre-Mauroux C, Occhiodoro T, Konig S, Salmon P, Bernheim L, Trono D: **Lentivector-mediated transfer of Bmi-1 and telomerase in muscle satellite cells yields a duchenne myoblast cell line with long-term genotypic and phenotypic stability.** *Hum Gene Ther* 2003, **14**:1525-1533.
32. Di Donna S, Renault V, Forestier C, Piron-Hamelin G, Thiesson D, Cooper RN, Ponsot E, Decary S, Amouri R, Hentati F, Butler-Browne GS, Mouly V:

Regenerative capacity of human satellite cells: the mitotic clock in cell transplantation. *Neurol Sci* 2000, **21(Suppl 5)**:S943-S951.
33. Seigneurin-Venin S, Bernard V, Moisset PA, Ouellette MM, Mouly V, Di Donna S, Wright WE, Tremblay JP: **Transplantation of normal and DMD myoblasts expressing the telomerase gene in SCID mice.** *Biochem Biophys Res Commun* 2000, **272**:362-369.
34. Seigneurin-Venin S, Bernard V, Tremblay JP: **Telomerase allows the immortalization of T antigen-positive DMD myoblasts: a new source of cells for gene transfer application.** *Gene Ther* 2000, **7**:619-623.
35. Song JS: **Adenovirus-mediated suicide SCLC gene therapy using the increased activity of the hTERT promoter by the MMRE and SV40 enhancer.** *Biosci Biotechnol Biochem* 2005, **69**:56-62.
36. Murasawa S, Llevadot J, Silver M, Isner JM, Losordo DW, Asahara T: **Constitutive human telomerase reverse transcripase expression enhances regenerative properties of endothelial progenitor cells.** *Circulation* 2002, **106**:1133-1139.
37. Watt FM: **Effect of seeding density on stability of the differentiated phenotype of pig articular chondrocytes in culture.** *J Cell Sci* 1988, **89(Pt 3)**:373-378.
38. Kudo T, Okumura M, Imaizumi K, Araki W, Morihara T, Tanimukai H, Kamagata E, Tabuchi N, Kimura R, Kanayama D, Fukumori A, Tagami S, Okochi M, Kubo M, Tanii H, Tohyama M, Tabira T, Takeda M: **Altered localization of amyloid precursor protein under endoplasmic reticulum stress.** *Biochem Biophys Res Commun* 2006, **344**:525-530.
39. Kudo T, Katayama T, Imaizumi K, Yasuda Y, Yatera M, Okochi M, Tohyama M, Takeda M: **The unfolded protein response is involved in the pathology of Alzheimer's disease.** *Ann N Y Acad Sci* 2002, **977**:349-355.
40. Yasuda Y, Kudo T, Katayama T, Imaizumi K, Yatera M, Okochi M, Yamamori H, Matsumoto N, Kida T, Fukumori A, Okumura M, Tohyama M, Takeda M: **FAD-linked presenilin-1 mutants impede translation regulation under ER stress.** *Biochem Biophys Res Commun* 2002, **296**:313-318.
41. Kozutsumi Y, Segal M, Normington K, Gething MJ, Sambrook J: **The presence of malfolded proteins in the endoplasmic reticulum signals the induction of glucose-regulated proteins.** *Nature* 1988, **332**:462-464.
42. Oyadomari S, Mori M: **Roles of CHOP/GADD153 in endoplasmic reticulum stress.** *Cell Death Differ* 2004, **11**:381-389.
43. Ni M, Lee AS: **ER chaperones in mammalian development and human diseases.** *FEBS Lett* 2007, **581**:3641-3651.

Pre-publication history
The pre-publication history for this paper can be accessed here:
http://www.biomedcentral.com/1471-2474/13/51/prepub

doi:10.1186/1471-2474-13-51
Cite this article as: Sato *et al.*: Human telomerase reverse transcriptase and glucose-regulated protein 78 increase the life span of articular chondrocytes and their repair potential. *BMC Musculoskeletal Disorders* 2012 13:51.

OPEN ACCESS Freely available online

PLoS one

Dynamics of Hepatitis B Virus Quasispecies in Association with Nucleos(t)ide Analogue Treatment Determined by Ultra-Deep Sequencing

Norihiro Nishijima[1], Hiroyuki Marusawa[1]*, Yoshihide Ueda[1], Ken Takahashi[1], Akihiro Nasu[1], Yukio Osaki[2], Tadayuki Kou[3], Shujiro Yazumi[3], Takeshi Fujiwara[4], Soken Tsuchiya[4], Kazuharu Shimizu[4], Shinji Uemoto[5], Tsutomu Chiba[1]

1 Department of Gastroenterology and Hepatology, Graduate School of Medicine, Kyoto University, Kyoto, Japan, **2** Department of Gastroenterology and Hepatology, Osaka Red Cross Hospital, Osaka, Japan, **3** Department of Gastroenterology and Hepatology, Tazuke Kofukai Medical Research Institute, Kitano Hospital, Osaka, Japan, **4** Department of Nanobio Drug Discovery, Graduate School of Pharmaceutical Sciences, Kyoto University, Kyoto, Japan, **5** Department of Surgery, Graduate School of Medicine, Kyoto University, Kyoto, Japan

Abstract

Background and Aims: Although the advent of ultra-deep sequencing technology allows for the analysis of heretofore-undetectable minor viral mutants, a limited amount of information is currently available regarding the clinical implications of hepatitis B virus (HBV) genomic heterogeneity.

Methods: To characterize the HBV genetic heterogeneity in association with anti-viral therapy, we performed ultra-deep sequencing of full-genome HBV in the liver and serum of 19 patients with chronic viral infection, including 14 therapy-naïve and 5 nucleos(t)ide analogue(NA)-treated cases.

Results: Most genomic changes observed in viral variants were single base substitutions and were widely distributed throughout the HBV genome. Four of eight (50%) chronic therapy-naïve HBeAg-negative patients showed a relatively low prevalence of the G1896A pre-core (pre-C) mutant in the liver tissues, suggesting that other mutations were involved in their HBeAg seroconversion. Interestingly, liver tissues in 4 of 5 (80%) of the chronic NA-treated anti-HBe-positive cases had extremely low levels of the G1896A pre-C mutant (0.0%, 0.0%, 0.1%, and 1.1%), suggesting the high sensitivity of the G1896A pre-C mutant to NA. Moreover, various abundances of clones resistant to NA were common in both the liver and serum of treatment-naïve patients, and the proportion of M204VI mutants resistant to lamivudine and entecavir expanded in response to entecavir treatment in the serum of 35.7% (5/14) of patients, suggesting the putative risk of developing drug resistance to NA.

Conclusion: Our findings illustrate the strong advantage of deep sequencing on viral genome as a tool for dissecting the pathophysiology of HBV infection.

Citation: Nishijima N, Marusawa H, Ueda Y, Takahashi K, Nasu A, et al. (2012) Dynamics of Hepatitis B Virus Quasispecies in Association with Nucleos(t)ide Analogue Treatment Determined by Ultra-Deep Sequencing. PLoS ONE 7(4): e35052. doi:10.1371/journal.pone.0035052

Editor: Antonio Bertoletti, Singapore Institute for Clinical Sciences, Singapore

Received November 17, 2011; **Accepted** March 8, 2012; **Published** April 16, 2012

Funding: This work was supported by JSPS Grant-in-aid for Scientific Research 21229009, 23390196, and Health and Labor Science Research Grants (H22-08) and Research on Hepatitis from the Ministry of Health, Labor and Welfare, Japan. (http://mhlw-grants.niph.go.jp/). The funders had no role in study design, data collection and analysis, decision to publish, or preparation of the manuscript.

Competing Interests: The authors have declared that no competing interests exist.

* E-mail: maru@kuhp.kyoto-u.ac.jp

Introduction

Hepatitis B virus (HBV) is a non-cytopathic DNA virus that infects approximately 350 million people worldwide and is a main cause of liver-related morbidity and mortality [1–3]. The absence of viral-encoded RNA-dependent DNA polymerase proofreading capacity coupled with the extremely high rate of HBV replication yields the potential to rapidly generate mutations at each nucleotide position within the entire genome [4]. Accordingly, a highly characteristic nature of HBV infection is the remarkable genetic heterogeneity at the inter- and intra- patient level. The latter case of variability as a population of closely-related but nonidentical genomes is referred to as viral quasispecies [5,6]. It is well recognized that such mutations may have important implications regarding the pathogenesis of viral disease. For example, in chronic infection, G to A point mutation at nucleotide (nt) 1896 in the pre-core (pre-C) region as well as A1762T and G1764A mutations in the core-promoter region are highly associated with HBeAg seroconversion that in general results in the low levels of viremia and consequent clinical cure [7–9]. In contrast, acute infection with the G1896A pre-C mutant represents a high risk for fulminant hepatic failure [10,11]. Although these facts clearly illustrate the clinical implications of certain viral mutation, increasing evidence strongly suggests that

the viral genetic heterogeneity is more complicated than previously thought [12,13].

The major goals of antiviral therapy in patients with HBV infection are to prevent the progression of liver disease and inhibit the development of hepatocellular carcinoma [14]. Oral nucleos(t)ide analogue (NA) have revolutionized the management of HBV infection, and five such antiviral drugs, including lamivudine, adefovir, entecavir, tenofovir, and telbivudine, are currently approved medications [15,16]. These agents are well-tolerated, very effective at suppressing viral replication, and safe, but one of the major problems of NA therapy is that long-term use of these drugs frequently causes the emergence of antiviral drug-resistant HBV due to substitutions at specific sites in the viral genome sequences, which often negates the benefits of therapy and is associated with hepatitis flares and death [16,17]. It is unclear whether viral clones with antiviral resistance emerge after the administration of antiviral therapy or widely preexist among treatment-naïve patients.

There has been a recent advance in DNA sequencing technology [18]. The ultra-deep sequencers allow for massively parallel amplification and detection of sequences of hundreds of thousands of individual molecules. We recently demonstrated the usefulness of ultra-deep sequencing technology to unveil the massive genetic heterogeneity of hepatitis C virus (HCV) in association with treatment response to antiviral therapy [19]. On the other hand, there are a few published studies in which this technology was used to characterize genetic HBV sequence variations [20–22]. Margeridon-Thermet et al reported that the 454 Life Science GS20 sequencing platform provided higher sensitivity for detecting drug-resistant HBV mutations in the serum of patients treated with nucleoside and nucleotide reverse-transcriptase inhibitors [20]. Solmone et al also reported the strong advantage conferred by the same platform to detect minor variants in the serum of patients with chronic HBV infection [21]. Although in these previous studies low-abundant drug-resistant variants were successfully detected, the analyses were focused on the reverse-transcriptase region of circulating HBV in the serum and thus the whole picture of HBV genetic heterogeneity as well as the *in vivo* dynamics of HBV drug resistant variants in response to anti-viral treatment remains to be clarified. Moreover, intrahepatic viral heterogeneity in patients that achieved the clearance of circulating HBV is largely unknown.

By taking the advantage of an abundance of genetic information obtained by utilizing the Illumina Genome Analyzer II (Illumina, San Diego, CA) as a platform of ultra-deep sequencing, we determined the whole HBV sequence in the liver and serum of patients with chronic HBV infection to evaluate viral quasispecies characteristics. Moreover, we investigated the prevalence of rare drug-resistant HBV variants as well as detailed dynamic changes in the viral genetic heterogeneity in association with NA administration. Based on the abundant genetic information obtained by ultra-deep sequencing, we clarified the precise prevalence of HBV clones with G1896A pre-C mutations in association with HBe serostatus in chronically infected patients with or without NA treatment. We also detected a variety of minor drug-resistant clones in treatment-naïve patients and their dynamic changes in response to entecavir administration, demonstrating the potential clinical significance of naturally-occurring drug-resistant mutations.

Materials and Methods

Ethics Statement

The Kyoto University ethics committee approved the study, and written informed consent for participation in this study was obtained from all patients. The study was conducted in accordance with the principles of the Declaration of Helsinki.

Patients

The liver tissues of 19 Japanese patients that underwent living-donor liver transplantation at Kyoto University due to HBV-related liver disease were available for viral genome analyses. These individuals included 13 men and 6 women, aged 41 to 69 years (median, 55.2 years) and all but one were infected with genotype C viruses. Participants comprised 19 patients with liver cirrhosis caused by chronic HBV infection, including 14 antiviral therapy-naïve cases (chronic-naïve cases) and 5 cases receiving NA treatment, with either lamivudine or entecavir (chronic-NA cases) (Table 1). Serum HBV DNA levels were significantly higher in chronic-naïve cases than in chronic NA cases (median serum HBV DNA levels were 5.6, and <2.6 log copies/ml, respectively, Table 1). Liver tissue samples were obtained at the time of transplantation, frozen immediately, and stored at −80°C until use. Serologic analyses of HBV markers, including hepatitis B surface antigen (HBsAg), antibodies to HBsAg, anti-HBc, HBeAg, and antibodies to HBeAg, were determined by enzyme immunoassay kits as described previously [23]. HBV DNA in the serum before transplantation was examined using a polymerase chain reaction (PCR) assay (Amplicor HBV Monitor, Roche, Branchburg, NJ). To examine the dynamics of viral quasispecies in response to anti-HBV therapy, paired serum samples of 14 treatment-naïve patients before and after administration of daily entecavir (0.5 mg/day) were subjected to further analyses on viral genome.

Direct population Sanger sequencing

DNA was extracted from the liver tissue and serum using a DNeasy Blood & Tissue Kit (Qiagen, Tokyo, Japan). To define the consensus reference sequences of HBV in each clinical specimen, all samples were first subjected to direct population Sanger sequencing using the Applied Biosystems 3500 Genetic Analyzer (Applied Biosystems, Foster City, CA). Oligonucleotide primers for the HBV genome were designed to specifically amplify whole viral sequences as two overlapping fragments using the sense primer 169_F and antisense primer 2847_R to yield a 2679-bp amplicon (amplicon 1), and the sense primer 685_F and antisense primer 443_R to yield a 2974-bp amplicon (amplicon 2; Table S1). HBV sequences were amplified using Phusion High-Fidelity DNA polymerase (FINZYMES, Espoo, Finland). All amplified PCR products were purified using the QIAquick Gel Extraction kit (Qiagen) after agarose gel electrophoresis and used for direct sequencing. The serum of a healthy HBV DNA-negative volunteer was used as a negative control.

Viral genome sequencing by massively-parallel sequencing

Massively-parallel sequencing with multiplexed tags was performed using the Illumina Genome Analyzer II as described [19]. The end-repair of DNA fragments, addition of adenine to the 3′ ends of DNA fragments, adaptor ligation, and PCR amplification by Illumina PCR primers were performed as described previously [24]. Briefly, the viral genome sequences were amplified by high-fidelity PCR using oligonucleotide primers as described above, sheared by nebulization using 32 psi N2 for 8 min, and then the sheared fragments were purified and concentrated using a QIAquick PCR purification Kit (Qiagen). Nucleotide overhangs resulting from fragmentation were then converted into blunt ends using T4 DNA polymerase and Klenow

Table 1. Characteristics of patients with chronic HBV infection analyzed in this study.

	Chronic-naïve (N = 14)	Chronic-NA (N = 5)
Age†	55.5 (41–69)	55.0 (49–68)
Sex (male/female)	9/5	4/1
Alanine aminotransaminase (IU/l)†	41 (10–74)	30 (15–65)
Total bilirubin (mg/dl)†	0.9 (0.5–31.1)	1.7 (0.6–4.5)
Platelet count ($\times 10^4$/mm^3)†	12.7 (3.3–27.6)	5.1 (3.6–11.3)
HBV genotype		
B	1	0
C	13	5
Viral load (log copies /ml)†	5.6 (<2.6–8.8)*	<2.6 (<2.6–5.3)*
HBe-serostatus (HBeAg+/HBeAb+)	8/6	0/5
Fibrosis		
F0–F2	6	0
F3–F4	8	5
Activity		
A0–A1	7	3
A2–A3	7	2

†Values are median (range).
*P = 0.042.
doi:10.1371/journal.pone.0035052.t001

enzymes, followed by the addition of terminal 3′ A-residues. An adaptor containing unique 6-bp tags, such as "ATCACG" and "CGATGT" (Multiplexing Sample Preparation Oligonucleotide Kit, Illumina), was then ligated to each fragment using DNA ligase. We then performed agarose gel electrophoresis of adaptor-ligated DNAs and excised bands from the gel to produce libraries with insert sizes ranging from 200 to 350 bp. These libraries were amplified independently using a minimal PCR amplification step of 18 cycles by Illumina PCR primers with Phusion High-Fidelity DNA polymerase. The DNA fragments were then purified with a MinElute PCR Purification Kit (Qiagen), followed by quantification using the NanoDrop 2000C (Thermo Fisher Scientific, Waltham, MA) to make a working concentration of 10 nM. Cluster generation and sequencing was performed for 64 cycles on the Illumina Genome Analyzer II according to the manufacturer's instructions. The obtained images were analyzed and base-called using GA pipeline software version 1.4 with the default settings provided by Illumina.

Genome Analyzer sequence data analysis

Using the high performance alignment software "NextGene" (SoftGenetics, State College, PA), the 64 base-pair reads obtained from the Genome Analyzer II were aligned with the reference sequences of 3215 bp that were determined by direct population Sanger sequencing of each clinical specimen. Reads with 90% or more bases matching a particular position of the reference sequences were aligned. Furthermore, two quality filters were used for sequencing reads: the reads with a median quality score of more than 30 and no more than 3 uncalled nucleotides were allowed anywhere in the 64 bases. Only sequences that passed the quality filters, rather than raw sequences, were analyzed and each position of the viral genome was assigned a coverage depth, representing the number of times the nucleotide position was sequenced.

Allele-specific quantitative real-time PCR and semiquantitative PCR to determine the relative proportion of G1896A pre-C mutant

To determine the relative proportion of the G1896A pre-C mutant, allele-specific quantitative real-time PCR was performed based on the previously described method [25,26]. Oligonucleotide primers were designed individually to amplify the pre-C region of wild-type and the G1896A pre-C mutant HBV. Three primers were used for this protocol, two allele-specific sense primers, 1896WT_F (for wild-type) and 1896MT_F (for the G1896A pre-C mutant), and one common antisense primer, 2037_R (Table S1). Quantification of wild-type and the G1896A pre-C mutant was individually performed by real-time PCR using a Light Cycler 480 and Fast Start Universal SYBR Master (Roche, Mannheim, Germany) [27]. The relative proportion of the G1896A pre-C mutant was determined to calculate the G1896A pre-C mutant/total HBV ratios. Performance of this assay was tested using mixtures of two previously described plasmids, pcDNA3-HBV-wt#1 and pcDNA3-HBV-G1896A pre-C mutant [28]. Semiquantitative PCR was performed using primers described above, then agarose gel electrophoresis was performed.

Statistical analysis

Results are expressed as mean or median, and range. Pretreatment values were compared using the Mann-Whitney U-test or the Kruskal Wallis H-test. *P* values less than 0.05 were considered statistically significant.

The viral quasispecies characteristics were evaluated by analyzing the genetic complexity based on the number of different sequences present in the population. Genetic complexity for each site was determined by calculating the Shannon entropy using the following formula:

$$Sn = -\frac{\sum_{i=1}^{n} fi(lnfi)}{N}$$

where n is the number of different species identified, fi is the observed frequency of a particular variant in the quasispecies, and N is the total number of clones analyzed [12,13]. The mean viral complexity in each sample was determined by calculating the total amounts of the Shannon entropy at each nucleotide position divided by the total nucleotide number (e.g., 3215 bases) of each HBV genome sequence.

Nucleotide sequence accession number

All sequence reads have been deposit in DNA Data Bank of Japan Sequence Read Archive (http://www.ddbj.nig.ac.jp/index-e.html) under accession number DRA000435.

Results

Validation of multiplex ultra-deep sequencing of the HBV genome

To differentiate true mutations from sequencing errors in the determined sequences, we first generated viral sequence data from the expression plasmid, pcDNA3-HBV-wt#1, encoding wild-type genotype C HBV genome sequences [28]. For this purpose, we determined the PCR-amplified HBV sequences derived from the expression plasmid using high-fidelity Taq polymerase to take the PCR-induced errors as well as sequencing errors into consideration. Viral sequences determined by the conventional Sanger method were used as reference sequences for aligning the amplicons obtained by ultra-deep sequencing. Three repeated ultra-deep sequencing generated a mean of 77,663 filtered reads, corresponding to a mean coverage of 38,234 fold at each nucleotide site (Table S2). Errors comprised insertions (0.00003%), deletions (0.00135%), and nucleotide mismatches (0.037%). The mean overall error rate was 0.034% (distribution of per-nucleotide error rate ranged from 0 to 0.13%) for the three control experiments, reflecting the error introduced by high-fidelity PCR amplification and by multiplex ultra-deep sequencing that remained after filtering out problematic sequences. We also confirmed that multiplex ultra-deep sequencing with and without the high-fidelity PCR amplification with HBV-specific primer sets showed no significant differences in the error rates on the viral sequence data (mean error rate 0.034% vs 0.043%). Accordingly, we defined the cut-off value in its current platform as 0.3%, a value nearly 1 log above the mean overall error rate.

Next, we performed additional control experiments to verify the detectability of the low abundant mutations that presented at a frequency of less than 0.3%. For this purpose, we introduced expression plasmids with a single-point mutation within that encoding a wild-type viral sequence with a ratio of 1:1000 and assessed the sensitivity and accuracy of quantification using high-fidelity PCR amplification followed by multiplex ultra-deep sequencing in association with the different coverage numbers (Table S3). Repeated control experiments revealed that the threshold for detecting low-abundant mutations at an input ratio of 0.10% among the wild-type sequences ranged between 0.11% and 0.24%, indicating that there was no significant difference in the detection rate or error rates under the different coverage conditions. Based on these results, the accuracy of ultra-deep sequencing in its current platform for detecting low-level viral mutations was considered to be greater than 0.30%.

Viral complexity of the HBV quasispecies in association with clinical status

To clarify HBV quasispecies in association with clinical status, we performed multiplex ultra-deep sequencing and determined the HBV full-genome sequences in the liver and serum with chronic HBV infection. First, we compared the sequences of the viral genome determined in the liver tissue with those in the serum and found no significant differences in the viral population between the liver and serum of the same individual. Indeed, the pattern and distribution of genetic heterogeneity of the viral nucleotide sequences in the liver tissue were similar to those observed in the serum of the same patient (Figure S1), suggesting that a similar pattern of viral heterogeneity was maintained in the liver and serum of patients with chronic HBV infection.

Next, we compared the viral heterogeneity in the liver of chronic-naïve and chronic-NA cases. A mean of 5,962,996 bp nucleotides in chronic-naïve cases and 4,866,783 bp nucleotides in chronic-NA cases were mapped onto the reference sequences, and an overall average coverage depth of 1,855 and 1.514 was achieved for each nucleotide site of the HBV sequences, respectively (Table 2). The frequencies of mutated positions and altered sequence variations detected in each viral genomic region are summarized in Table 2. The overall mutation frequency of the total viral genomic sequences was determined to be 0.87% in chronic-naïve cases and 0.69% in chronic-NA cases. Most genomic changes observed in viral variants were single base substitutions, and the genetic heterogeneity of the viral nucleotide sequences was equally observed throughout the individual viral genetic regions, including the pre-surface (preS), S, pre-core~core (preC-C), and X (Table 2). Consistent with the findings obtained from the viral mutation analyses, the overall viral complexity determined by the Shannon entropy value was 0.047 in chronic-naïve and 0.036 in chronic-NA cases, and the viral complexity was equally observed throughout the individual viral genetic region (Figure 1A). Among chronic-naïve cases, we observed no significant differences in the viral complexity in HBV DNA level, age, or degree of fibrosis (Figure 1B).

High sensitivity of the G1896A pre-C mutant to nucleos(t)ide analogues

Emergence of G1896A mutation in the pre-C region, and A1762T and G1764A mutations in the core-promoter region is well known to be associated with HBe-seroconversion [7–9]. We then evaluated the prevalence of these three mutations in the chronically HBV-infected liver, in association with HBe serologic status and the NA treatment history. In chronic-naive cases, 6 and 8 patients showed the pre- and post- HBeAg seroconversion status, respectively (Table 3). The mean prevalence of the G1896A pre-C mutant in HBeAg-positive cases was lower than that in the HBeAg-negative cases (27.4% and 46.5%, respectively). Importantly, however, 4 of 8 HBeAg-negative cases showed a relatively low prevalence of the G1896A pre-C mutant (Liver #8, #12, #13, #14), and all but one case (Liver #10) showed a high prevalence of the A1762T and G1764A mutations, irrespective of HBe serologic status and NA treatment history (Table 3). These findings suggested that other mutations except G1896A, A1762T and G1764A were also involved in the HBeAg seroconversion status. Notably, liver tissues of all but one (Liver #17) chronic-NA cases showed extremely low levels of the G1896A pre-C mutant (0.0, 0.0, 0.1, and 1.1%), suggesting the high sensitivity of the G1896A pre-C mutant to NA (Table 3).

To confirm the difference of the sensitivity to NA between the wild-type and the G1896A pre-C mutant, we examined the dynamic changes of the relative proportion of the G1896A pre-C mutant in the serum of 14 treatment-naïve patients before and after entecavir administration. Consistent with the findings obtained by ultra-deep sequencing, quantitative real-time PCR revealed that entecavir administration significantly reduced the proportion of the G1896A pre-C mutant in 13 of 14 cases (92.9%)

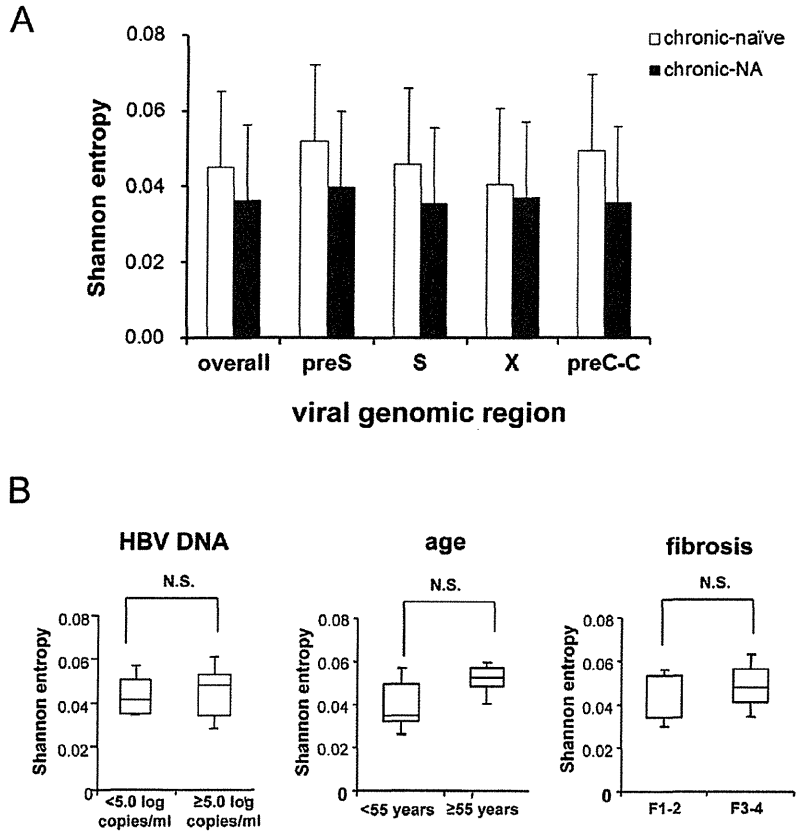

Figure 1. Viral complexity of the HBV quasispecies in association with clinical status. (A) The Shannon entropy values for each viral genomic region were determined in the liver of chronic-naïve and chronic-NA cases. (B) Among the chronic-naïve cases, the Shannon entropy values are shown for patients with serum HBV DNA levels less than 5.0 log copies/ml (<5.0) and greater than 5.0 log copies/ml (≥5.0) (left panel), patients under the age of 55 years (<55) and over the age of 55 (≥55) (middle panel), and patients with low (F1–2) and high (F3–4) liver fibrosis levels (right panel). preS: pre-surface, preC-C: precore~core N.S.: not significant.
doi:10.1371/journal.pone.0035052.g001

Table 2. The frequency of mutation rate and the Shannon entropy in each viral genome region.

	Liver	
	Chronic-naïve (N=14)	Chronic-NA (N=5)
Average aligned reads	93,172	76,043
Average aligned nucleotides	5,962,996	4,866,783
Average coverage	1,855	1,514
Mutation rate (%)		
Overall	0.87	0.69
preS	0.92	0.81
S	0.96	0.71
preC-C	1.05	0.72
X	0.63	0.61
Shannon entropy	0.047	0.036

Mutation rate (%): the ratio of total different nucleotides from the reference sequence to total aligned nucleotides.
preS: pre-surface, preC-C: pre-core~core.
doi:10.1371/journal.pone.0035052.t002

irrespective of their HBeAg serostatus, while the G1896A pre-C mutant were detectable in substantial proportion before treatment in all cases (Figure 2A, 2B and 2C; $p = 0.001$). These results further support the findings that HBV clones comprising the G1896A mutation were more sensitive to NA than those with wild-type sequences.

Prevalence of drug-resistant HBV clones in the liver of treatment-naïve patients

Increasing evidence suggests that drug-resistant viral mutants can be detected in the serum of treatment-naïve patients with chronic HBV infection [20,21]. Thus, we next determined the actual prevalence of spontaneously-developed drug-resistant mutants in chronically-infected liver of treatment-naïve patients to evaluate whether NA treatment potentiates the expansion of drug-resistant clones. The drug-resistant mutations examined included two mutations resistant to lamivudine and entecavir, four mutations resistant to entecavir, and three mutations resistant to adefovir [16,17]. Based on the detection rate of the low-level viral clones determined by the control experiments, we identified the drug-resistant mutants present in each specimen at a frequency of more than 0.3% among the total viral clones. Based on these criteria, at least one resistant mutation was detected in the liver of all of the chronic-naïve cases with chronic HBV infection (Table 4).

Table 3. The prevalence of G1896A mutation in the pre-C region, and A1762T and G1764A mutations in the core-promoter region in the liver of patients chronically infected with HBV.

			Mutation Frequency					
	HBeAg/HBeAb	NA (duration of treatment)	G1896A (Pre C)		A1762T (CP)		G1764A (CP)	
Chronic-naive								
Liver #1	+/−	-	640/1652	(38.7)	1647/1941	(84.9)	1683/1979	(85.0)
Liver #2	+/−	-	9/596	(1.5)	682/687	(99.3)	683/689	(99.1)
Liver #3	+/−	-	273/672	(40.6)	767/769	(99.7)	757/760	(99.6)
Liver #4	+/−	-	204/701	(29.1)	610/625	(97.6)	602/621	(96.9)
Liver #5	+/−	-	27/152	(17.8)	249/250	(99.6)	245/248	(98.8)
Liver #6	+/−	-	228/621	(36.7)	727/729	(99.7)	743/744	(99.9)
Liver #7	−/+	-	740/1193	(62.0)	1908/1913	(99.7)	1888/1913	(98.7)
Liver #8	−/+	-	111/1892	(5.9)	2321/2325	(99.8)	2335/2339	(99.8)
Liver #9	−/+	-	10935/10944	(99.9)	12019/12032	(99.9)	12163/12170	(99.9)
Liver #10	−/+	-	4554/4593	(99.2)	1/5191	(0)	4/5188	(0.1)
Liver #11	−/+	-	811/921	(88.1)	1234/1236	(99.8)	1226/1228	(99.8)
Liver #12	−/+	-	93/1265	(7.4)	1234/1234	(100)	1228/1229	(99.9)
Liver #13	−/+	-	83/877	(9.5)	1465/1529	(95.8)	1485/1549	(95.9)
Liver #14	−/+	-	0/717	(0)	1078/1410	(76.5)	1089/1414	(77.0)
Chronic-NA								
Liver #15	−/+	LAM (156w)	0/390	(0)	441/453	(97.4)	435/448	(97.1)
Liver #16	−/+	ETV (1w)	0/1399	(0)	1624/1632	(99.5)	1625/1630	(99.7)
Liver #17	−/+	LAM (144w)	345/816	(42.3)	988/991	(99.7)	994/994	(100)
Liver #18	−/+	LAM (98w)	2/3963	(0.1)	1015/1188	(85.4)	1190/1194	(99.7)
Liver #19	−/+	LAM (11w)	48/4214	(1.1)	3438/3456	(99.5)	3446/3462	(99.5)

Values in parenthesis show mutation frequency (%): the ratio of total mutant clones to total aligned coverage at each nucleotide sites.
NA: nucleotide analogue, pre C: precore, CP: core promoter, LAM: lamivudine, ETV: entecavir.
doi:10.1371/journal.pone.0035052.t003

The prevalence of the 9 drug-resistant mutations detected by ultra-deep sequencing in 14 chronic-naïve cases ranged from 0.3% to 30.0%, indicating that the proportion of resistant mutations substantially differed in each case. The most commonly detected mutation was M204VI (9 cases) and M250VI (11 cases), which were resistant to lamivudine and entecavir, and entecavir, respectively. Other mutations resistant to adefovir were detected in 7 (50.0%) and 3 (21.4%) cases at A181TV and N236T, respectively (Table 4).

Nine (64.2%) chronic-naïve cases possessed the M204VI mutants in their liver tissues and the proportion of mutant clones among the totally infected viruses ranged from 0.3% to 1.1% among the M204VI mutant-positive patients. In chronic-NA cases, 4 of 5 (80.0%) liver tissues harbored the M204VI mutants with the proportion among the totally infected viruses ranging from 0.4% to 18.7% (Table 4), while the mean serum HBV DNA was suppressed below 2.6 log copies/ml (Table 1). These results suggest that the mutant HBV clones comprising various drug-resistant mutations could latently exist even in the liver of NA treatment-naïve cases.

Expansion of drug-resistant HBV clones harboring M240VI mutations in response to NA administration

To clarify the risk of latent expansion of drug-resistant mutations due to NA treatment, we next examined the early dynamic changes of the prevalence of M204VI mutants in the serum of treatment-naïve patients in response to entecavir treatment. Ultra-deep sequencing provided a mean 40,791- and 38,823-fold coverage of readings, which were mapped to the M204VI nucleotide position at the YMDD sites of each reference sequence in patients before and after entecavir treatment.

Five of 14 (35.7%) patients harbored the M204VI mutations prior to entecavir treatment. Although the serum HBV DNA levels were significantly reduced in response to entecavir in all cases, the M204VI mutant clones were detected in 9 cases (64.3%) after entecavir administration (Table 5). Notably, one patient (Serum #3) who harbored the M240VI mutant clones at baseline had a relatively large expansion of drug-resistant clones among the total viral population in a time-dependent manner in response to entecavir treatment (Table 5). Similarly, M240VI mutant clones became detectable after entecavir administration in four patients (Serum #1, #7, #12, #13) that harbored no resistant mutants at baseline (Table 5). We found no correlation between the degree of the increase in the relative prevalence of M204VI mutant clones and that of the reduction in serum HBV DNA levels. Although only a limited number of patients exhibited a substantial increase in M204VI mutant clones after administration of anti-viral therapy, our findings might suggest that entecavir treatment latently causes selective survival of drug-resistant mutants in treatment naïve patients with chronic HBV infection.

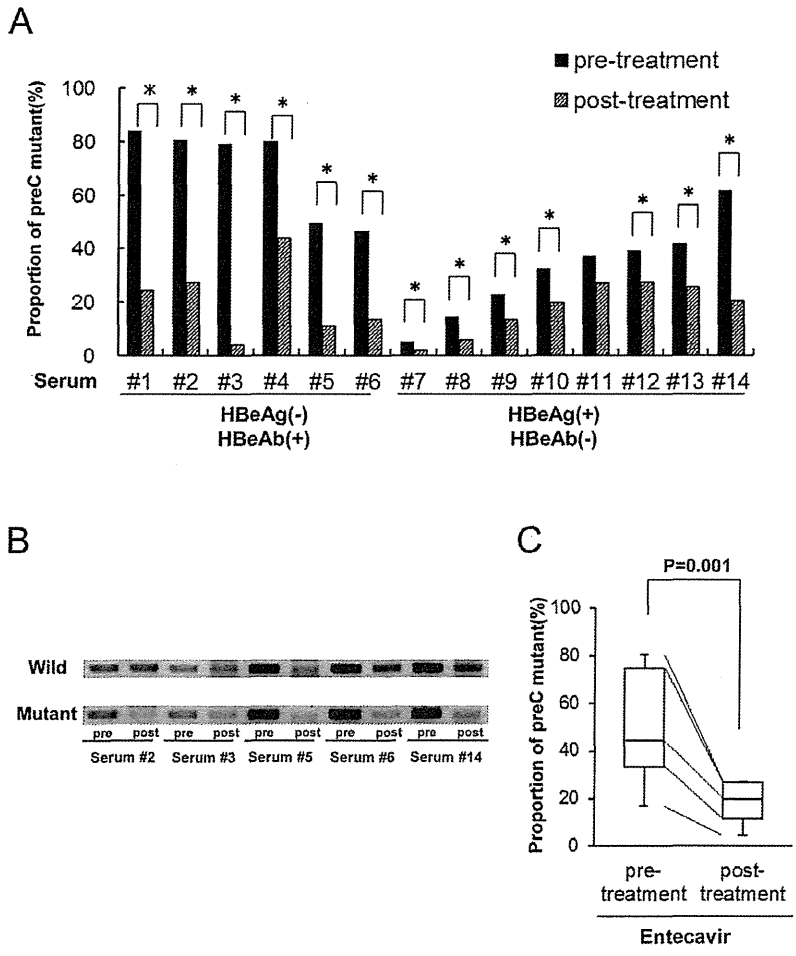

Figure 2. The reduction in the relative proportion of the G1896A pre-C mutant clones after entecavir administration. (A) The relative proportion of the G1896A pre-C mutant was determined in the serum of treatment-naïve patients pre- and post-entecavir administration using quantitative real-time PCR. Serum #1~6 were HBeAg-negative and HBeAb-positive, and Serum #7~14 were HBeAg-positive and HBeAb-negative before treatment. *: $p<0.05$ (B) Semiquantitative PCR analysis was performed using primers specific to the wild-type (upper panel) or G1896A pre-C mutant (lower panel) pre- and post-entecavir administration. A representative result from 5 cases is shown. (C) The relative proportion of the G1896A pre-C mutant was compared in 14 treatment-naïve patients between pre- and post-entecavir administration.
doi:10.1371/journal.pone.0035052.g002

Discussion

Direct population sequencing is the most common method for detecting viral mutations [29]. Conventional sequencing techniques, however, are not efficient for evaluating large amounts of genetic information of the viruses. Newly developed ultra-deep sequencing technology have revolutionized genomic analyses, allowing for studies of the dynamics of viral quasispecies as well as rare genetic variants of the viruses that cannot be detected using standard direct population sequencing techniques [30,31]. The sensitivity of ultra-deep sequencing analysis is primarily limited by errors introduced during PCR amplification and the sequencing reaction, thus it is a challenge to distinguish rare variants from sequencing artifacts. In the present study, we optimized the ultra-deep sequencing with a multiplex-tagging method and reproducibly detected variants within HBV quasispecies that were as rare as 0.3%. Based on this ultra-deep sequencing platform, we determined the abundant genetic heterogeneity of HBV at the intra- and inter-individual levels.

Because of its ability to handle abundant viral genome information, ultra-deep sequencing allowed us to evaluate low-abundant virus variants of patients with chronic HBV infection in detail. It is widely accepted that HBe seroconversion is highly associated with the emergence of G1896A pre-C and/or A1762T and G1764A core promoter mutant clones [7–9]. Unexpectedly, however, our results showed a diverse range of G1896A frequency (0–99.9%) in HBeAg-negative subjects and a high prevalence of core promoter mutations, irrespective of HBe serostatus. Consistent with our observation, previous studies utilizing conventional sequencing methods reported that the frequency of the G1896A pre-C mutant ranged from 12% to 85% [32]. All but one patient (Liver #10) showing a predominance of A1762T and G1764A were infected with genotype C, while patient#10 was infected with genotype B. Because A1762T and G1764A are reported to be significantly more frequent in genotype C [33], the difference in the prevalence of A1762T and G1764A in our study might be a reflection of the viral HBV genotype rather than HBe serostatus. Further investigation of the actual prevalence of these mutations

Table 4. The prevalence of the 9 drug-resistant mutations detected by ultra-deep sequencing derived from liver tissue.

	M204V/I		L180M		T184S/A/I/ L/G/C/M		S202C/G/I		I169T	
Drugs	**LAM/ETV**		**LAM/ETV**		**ETV**		**ETV**		**ETV**	
Chronic-naive										
Liver #1	**27/5421**	**(0.5%)**	2/3694	(-)	9/3886	(-)	5/5613	(-)	5/3784	(-)
Liver #2	**35/5344**	**(0.7%)**	0/538	(-)	1/563	(-)	17/6340	(-)	0/512	(-)
Liver #3	**13/1363**	**(1.0%)**	0/304	(-)	1/358	(-)	1/1379	(-)	0/264	(-)
Liver #4	11/5113	(-)	0/556	(-)	**2/547**	**(0.4%)**	11/5133	(-)	0/639	(-)
Liver #5	**2/117**	**(1.1%)**	0/409	(-)	1/380	(-)	1/189	(-)	1/474	(-)
Liver #6	12/8451	(-)	0/309	(-)	0/328	(-)	22/8457	(-)	0/334	(-)
Liver #7	**10/3098**	**(0.3%)**	1/1547	(-)	3/1477	(-)	8/3161	(-)	0/1621	(-)
Liver #8	**13/2442**	**(0.5%)**	1/2378	(-)	6/2312	(-)	1/2564	(-)	1/2507	(-)
Liver #9	**67/13879**	**(0.5%)**	2/5443	(-)	2/5107	(-)	6/13804	(-)	0/5650	(-)
Liver #10	16/7400	(-)	0/3524	(-)	3/3283	(-)	5/7113	(-)	0/3492	(-)
Liver #11	0/412	(-)	1/1328	(-)	**1/295**	**(0.3%)**	0/425	(-)	3/4729	(-)
Liver #12	**4/1098**	**(0.4%)**	1/1389	(-)	0/1272	(-)	2/1102	(-)	0/1544	(-)
Liver #13	**8/2476**	**(0.3%)**	1/2192	(-)	3/2085	(-)	4/2529	(-)	4/5029	(-)
Liver #14	5/3713	(-)	0/2009	(-)	4/1925	(-)	2/3820	(-)	5/3784	(-)
Chronic-NA										
Liver #15	0/339	(-)	0/49	(-)	0/49	(-)	0/338	(-)	0/40	(-)
Liver #16	**28/7278**	**(0.4%)**	0/4403	(-)	6/4053	(-)	14/7556	(-)	6/6084	(-)
Liver #17	**177/945**	**(18.7%)**	0/1059	(-)	0/1009	(-)	0/945	(-)	0/1051	(-)
Liver #18	**13/2655**	**(0.5%)**	0/1239	(-)	0/1185	(-)	**10/2708**	**(0.4%)**	0/1332	(-)
Liver #19	**80/6795**	**(1.2%)**	0/3168	(-)	2/2971	(-)	3/6734	(-)	0/3384	(-)

	M250V/I		A181T/V		N236T		P237H	
Drugs	**ETV**		**ADV**		**ADV**		**ADV**	
Chronic-naive								
Liver #1	**23/2719**	**(0.9%)**	10/3755	(-)	4/4210	(-)	2/4139	(-)
Liver #2	**9/2079**	**(0.4%)**	**2/549**	**(0.4%)**	1/1144	(-)	1/1188	(-)
Liver #3	**10/1699**	**(0.6%)**	**1/298**	**(0.3%)**	3/1636	(-)	1/1666	(-)
Liver #4	**3/388**	**(0.8%)**	**3/549**	**(0.5%)**	0/560	(-)	0/533	(-)
Liver #5	**2/91**	**(2.2%)**	1/409	(-)	0/55	(-)	0/60	(-)
Liver #6	0/214	(-)	**6/305**	**(2.0%)**	**1/294**	**(0.3%)**	0/257	(-)
Liver #7	**7/1289**	**(0.5%)**	4/1531	(-)	**24/2738**	**(0.9%)**	1/2692	(-)
Liver #8	2/1117	(-)	**689/2336**	**(29.5%)**	2/1713	(-)	0/1639	(-)
Liver #9	**27/7325**	**(0.4%)**	**38/5334**	**(0.7%)**	1/6607	(-)	4/6702	(-)
Liver #10	**12/3815**	**(0.3%)**	0/3454	(-)	**13/3245**	**(0.4%)**	2/3272	(-)
Liver #11	**1/199**	**(0.5%)**	1/972	(-)	0/251	(-)	0/251	(-)
Liver #12	**2/672**	**(0.3%)**	**408/1362**	**(30.0%)**	0/598	(-)	0/597	(-)
Liver #13	1/947	(-)	2/2160	(-)	0/1406	(-)	1/1374	(-)
Liver #14	**23/2719**	**(0.9%)**	10/3755	(-)	4/4210	(-)	2/4139	(-)
Chronic-NA								
Liver #15	**1/303**	**(0.3%)**	**2/49**	**(4.1%)**	0/377	(-)	0/384	(-)
Liver #16	1/922	(-)	0/4403	(-)	1/1597	(-)	3/1572	(-)
Liver #17	0/755	(-)	1/1050	(-)	0/698	(-)	**145/698**	**(20.8%)**
Liver #18	1/1464	(-)	2/1206	(-)	0/3156	(-)	0/3107	(-)
Liver #19	8/3834	(-)	**16/3128**	**(0.5%)**	0/3372	(-)	0/3428	(-)

(-): mutant clones less than 0.3% among total clones at each nucleotide sites.
LAM: lamivudine, ADV: adefovir, ETV: entecavir.
doi:10.1371/journal.pone.0035052.t004